Advances in Difference Equations
a SpringerOpen Journal

RESEARCH Open Access

Solutions of fractional order differential equations modeling temperature distribution in convective straight fins design

Ashfaq Ahmad[1], Muhammad Sulaiman[1*] and Poom Kumam[2,3*]

*Correspondence:
msulaiman@awkum.edu.pk;
poom.kum@kmutt.ac.th
[1]Department of Mathematics, Abdul Wali Khan University, Mardan 23200, KP, Pakistan
[2]KMUTT Fixed Point Research Laboratory, KMUTT-Fixed Point Theory and Applications Research Group, SCL 802 Fixed Point Laboratory, Department of Mathematics, Faculty of Science, King Mongkut's University of Technology Thonburi (KMUTT), 126 Pracha Uthit Rd., Bang Mod, Thung Khru, Bangkok 10140, Thailand
Full list of author information is available at the end of the article

Abstract

In this paper, the problem of temperature distribution for convective straight fins with constant and temperature-dependent thermal conductivity is solved by using artificial neural networks trained by the biogeography-based heterogeneous cuckoo search (BHCS) algorithm. We have solved the integer and noninteger order energy balance equation in order to analyse the temperature distribution in convective straight fins. We have compared our results with homotopy perturbation method (HPM), variational iteration method (VIM), and homotopy perturbation Sumudu transform method (HPSTM). The results show that the ANN–BHCS algorithm gives better results than other analytical techniques. We have further checked the efficiency of the ANN–BHCS algorithm by using the performance metrics MAD, TIC, and ENSE. We have calculated the values of MAD, TIC, and ENSE for case 1 of the problem, and histograms of these metrics show the efficiency of our algorithm.

Keywords: Fractional order differential equations; Design engineering; Mathematical models; Intelligent computing techniques; Artificial neural networks; Heuristic optimization techniques

1 Introduction

A vast number of problems which model physical phenomena, for example heat transfer, involve the nonlinear function [1]. In mechanical engineering, heat transfer is a very common science because in various objects it can be required. The problems of improvement of heat transfer are solved on an extended surface which is known as fin. The heat transfer mechanism of fin is to conduct heat through its thermal conduction from the source of heat to the fin's surface, and then heat is dissipated into the air through the effects of thermal radiation and convection. In addition to traditional uses, like heat exchangers, compressors, and engines with internal combustion, fins also demonstrate efficiency in the systems of heat rejection and cooling of electronic parts of space vehicles [2, 3]. A broad analysis on this subject was presented in [4] by Kern and Kraus. By using the homotopy perturbation technique, Domairry and Fazeli investigated the efficacy of the convective

fins in [5]. The heat transfer dynamics of fins in space radiator and one-dimensional radiation fins are further investigated in [6–8]. The system of heat-rejecting comprising parallel tubes connected by web plates has been studied by Bartas and Sellers [9]. In [10], Hug and Aziz used a perturbation-based technique to find the closed form solutions for straight convective fin with thermal conductivity which is dependent on temperature. To find analytical solution for dimensionless temperature and investigate the efficiency of the fin having thermal conductivity dependent on temperature, Arslanturk [11, 12] used Adomian decomposition technique.

In recent years, studying the heat transfer on extended surfaces has become very pivotal with growing importance of performance of heat transfer fins having lower volumes, weights, initial and operating costs of the systems [11]. In addition to the developments in standard methods of numerical computation, a new methodology, which is known as homotopy perturbation Sumudu transformation technique, was proposed to analyze less or strongly nonlinear systems. HPSTM has recently been used for solution of nonlinear fractional equation of gas dynamics and some other physical phenomena [13]. Sumudu transform method, homotopy perturbation method (HPM), and He's polynomials are combined to design the HPSTM technique [14]. Fractional calculus [15, 16] is a branch of applied mathematics which deals with arbitrary order differentiation and integration. It has found many applications in different areas of science and engineering over the last three decades [17–20]. The HPSTM is used for the solution of energy balance equation of fractional order [21]. More works on analytical and numerical techniques for the solving integer and fractional differential equations are available in [22–51].

In this work, we have designed a hybrid of ANNs and biogeography-based heterogeneous cuckoo search algorithm (BHCS) for the solution of integer and fractional order energy balance equation in order to analyze the temperature distribution in convective straight fins. We have named our algorithm the ANN–BHCS algorithm. We have analyzed seven cases of the problems and the results are compared with other techniques such as HPM, VIM, and HPSTM [6, 21, 52]. The results show that the ANN–BHCS algorithm is better than other techniques in terms of obtaining the solutions with high accuracy. We have further tested the efficiency of the ANN–BHCS algorithm by utilizing the performance metrics MAD, TIC, and ENSE.

Key contributions of our work are given below:

- We have designed a hybrid technique of ANNs and BHCS which is named ANN–BHCS algorithm, see Fig. 1. The ANN model is designed for the solution of integer and fractional order differential equations, see Fig. 3.
- The problem of temperature distribution in convective straight fin is analyzed, see Fig. 2. Three integer order and four fractional order cases of the problem are considered.
- To validate the results obtained by the ANN–BHCS algorithm, we have compared it with analytical techniques such as HPM, VIM, and HPSTM.
- To check the quality of the solutions and efficiency of the algorithm, we have calculated three performance metrics which are mean absolute deviation (MAD), Theil's inequality coefficient (TIC), and error in Nash–Sutcliffe efficiency ENSE.

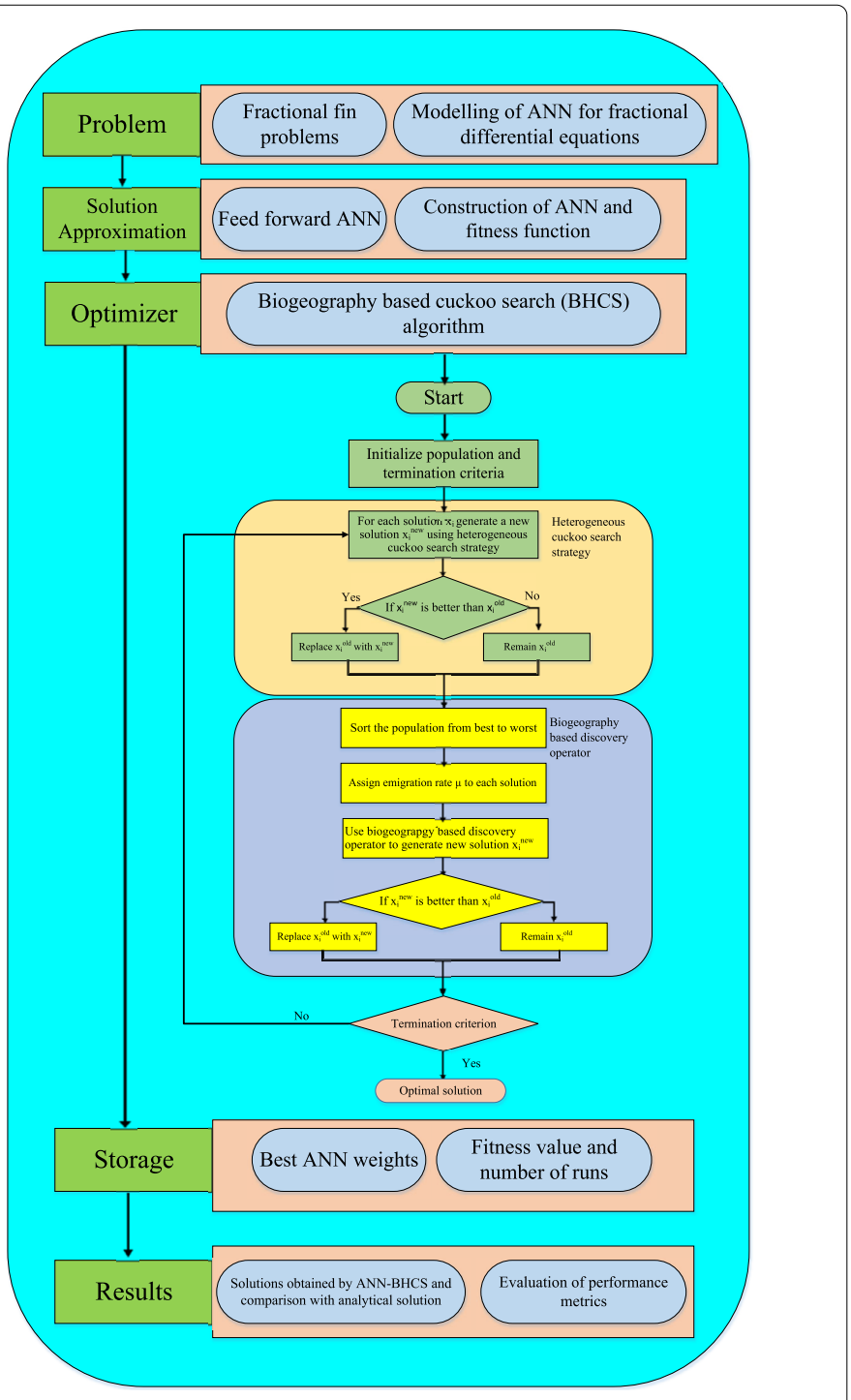

Figure 1 Graphical abstract for paper

2 Straight convective fins with temperature-dependent thermal conductivity

Consider a straight convective fin having thermal conductivity dependent on temperature, and it has an arbitrary constant area of cross section A_c, length b, and perimeter P, and the heat transfer coefficient is denoted by h. The fin is associated with the temperature T at the base surface, and extends into temperature T_a of the fluid. The geometry of the

Figure 2 Geometry of the straight fin

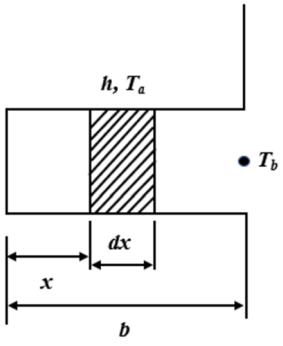

straight fin is given in Fig. 2. The one-dimensional energy balance equation is given by [52, 53]

$$A_c \frac{d}{dx}\left[k(T)\frac{dT}{dx}\right] - Ph(T - T_a) = 0. \tag{1}$$

The thermal conductivity of fin's material is considered as a linear function according to Eq. (2),

$$k(T) = k_a\big[1 + \lambda(T - T_a)\big], \tag{2}$$

where k is the parameter defining the variation of the thermal conductivity and k_a is the thermal conductivity at the ambient fluid temperature of the fin.

Introducing the dimensionless parameters:

$$\theta = \frac{T - T_a}{T_b - T_a}, \qquad \xi = \frac{x}{b}, \qquad \beta = \lambda(T_b - T_a) \quad \text{and} \quad \psi = \left(\frac{hPb^2}{k_a A_c}\right)^{1/2}. \tag{3}$$

Now Eq. (1) reduces to the following equation:

$$\frac{d^2\theta}{d\xi^2} + \beta\theta\frac{d^2\theta}{d\xi^2} + \beta\left(\frac{d\theta}{d\xi}\right)^2 - \psi^2\theta = 0; \quad 0 \le \xi \le 1, \tag{4}$$

with the following boundary conditions:

$$\theta'(0) = 0 \quad \text{and} \quad \theta(1) = 1. \tag{5}$$

The computational domain $0 \le x \le b$ is transformed to $0 \le \xi \le 1$ by introducing the dimensionless parameters given in Eq. (3).

To understand the anomalous behavior of this system, we fractionalize the energy balance Eq. (4) into fractional order ($\nu > 0$) as follows in order to find fin temperature in straight fins:

$$\frac{d^\nu\theta}{d\xi^\nu} + \beta\theta\frac{d^2\theta}{d\xi^2} + \beta\left(\frac{d\theta}{d\xi}\right)^2 - \psi^2\theta = 0; \quad 1 < \nu \le 2 \text{ and } 0 \le \xi \le 1, \tag{6}$$

with the following boundary conditions as in Eq. (5).

3 Basic definitions

This section consists of some definitions and important relations from fractional calculus that have been used in the construction of ANN for FDEs. Fractional derivatives and integrals have been expressed in different ways in literature, i.e., Riemann–Liouville, Caputo, Erdélyi–Kober, Hadamard, Grünwald–Letnikov, and Riesz type etc. In standard fractional calculus, equivalence of these definitions for some functions has been given [15, 54, 55]. All of these definitions have their own importance and advantages in different kinds of problems in mathematics. Definitions of Riemann–Liouville and Caputo fractional derivatives are given below.

Definition 1 (The fractional order Riemann–Liouville integral and derivative) The integral of fractional order $\nu > 0$ can be written as [16]

$$\left(I^{\nu} f\right)(x) = \frac{1}{\Gamma(\alpha)} \int_0^x (x-\tau)^{\nu-1} f(\tau)\, d\tau, \tag{7}$$

$$\left(I^{0} f\right)(x) = f(x). \tag{8}$$

Here, I^{ν} shows the fractional integral of order ν. The fractional derivative of order $\nu > 0$ is normally given as

$$\left(D^{\nu} f\right)(x) = \left(\frac{d}{dx}\right)^{n} \left(I^{n-\nu} f\right)(x) \quad (n-1 < \nu \leq n). \tag{9}$$

Here, D^{ν} represents the fractional derivative of order ν and n is an integer.

Definition 2 (Caputo fractional derivatives) There are some limitations of the definition of fractional derivatives given by Riemann–Liouville, when it is used for modeling of some real world phenomena related to differential equations of fractional order. Therefore, a modified definition for fractional differential operator D^{ν} is introduced by Caputo [16, 56]:

$$\left(D^{\nu} f\right)(x) = I^{n-\nu} \frac{d^n}{dx^n} f(x) = \frac{1}{\Gamma(n-\nu)} \int_0^x (x-\tau)^{n-\nu-1} f^{(n)}(\tau)\, d\tau \quad (n-1 < \nu \leq n), \tag{10}$$

where I^{ν} is given in Eq. (3). Caputo integral operator is given by

$$\left(I^{\nu} D^{\nu} f\right)(x) = f(x) - \sum_{k=0}^{n-1} f^{k}(0) \frac{x^k}{k!} \quad (n-1 < \nu \leq n). \tag{11}$$

The ordinary derivative followed by a fractional integral gives the Caputo fractional derivative, while the calculation in reverse order gives the Riemann–Liouville derivative. Using Caputo fractional derivative, we can use the traditional homogeneous and nonhomogeneous initial/boundary conditions occurring in general applications. However, for homogeneous initial conditions, Riemann–Liouville and Caputo formulations coincide [16, 57].

Definition 3 (Mittag-Leffler function (MLF)) The Mittag-Leffler function (MLF) is one of the most important functions having widespread applications in fractional calculus. It

plays an important role in the solution of differential equations of integer and fractional orders because of its exponential nature.

The classical MLF has the definition as given below [58]:

$$E_{\alpha}(x) = \sum_{k=0}^{\infty} \frac{x^k}{\Gamma(\alpha k + 1)} \quad (\alpha > 0). \tag{12}$$

It becomes the exponential function when $\alpha = 1$. The MLF function with two parameters α and β is as follows:

$$E_{\alpha,\beta}(t) = \sum_{k=0}^{\infty} \frac{t^k}{\Gamma(\alpha k + \beta)} \quad (\alpha > 0, \beta > 0). \tag{13}$$

For $\beta = 1$, it becomes a standard MLF function.

4 Solution methodology

4.1 ANN modeling

This section presents the mathematical modeling of artificial neural networks (ANN) for differential equations of fractional order. Neural networks modeling has already been implemented for solving integer order differential equations. Now, we model the ANN to find the solution for fractional order differential equations.

The exponential function is used as an activation function for ANN. It has the capability to approximate the functions and its fractional derivative is also calculated with terms represented by classical MLF. The fractional derivative of an exponential function can be written as

$$\frac{d^{\nu}}{dx^{\nu}} e^{\lambda x} = x^{-\nu} E_{1,1-\nu}(\lambda x). \tag{14}$$

Approximate solution for the problem considered in this research and its ν order derivative is given by

$$\hat{\theta}(\xi) = \sum_{i=1}^{m} \alpha_i e^{\omega_i \xi + \beta}, \tag{15}$$

$$\frac{d^{\nu}}{d\xi^{\nu}} \hat{\theta}(\xi) = \sum_{i=1}^{m} \alpha_i e^{\beta_i} \xi^{-\nu} E_{1,1-\nu}(\omega_i \xi). \tag{16}$$

Equations (15) and (16) are used to approximate a solution of the fractional order differential equation given in Eq. (6). The neural networks architecture for fractional differential equations is given in Fig. 3. The objective function for the problem considered in this paper is given by

$$\min \quad E = E_1 + E_2, \tag{17}$$

where E_1 and E_2 are given by

$$E_1 = \frac{1}{N+1} \sum_{m=0}^{N} \left(\frac{d^{\nu}\hat{\theta}}{d\xi^{\nu}} + \beta\hat{\theta} \frac{d^2\hat{\theta}}{d\xi^2} + \beta \left(\frac{d\hat{\theta}}{d\xi} \right)^2 - \psi^2 \hat{\theta} \right)^2, \tag{18}$$

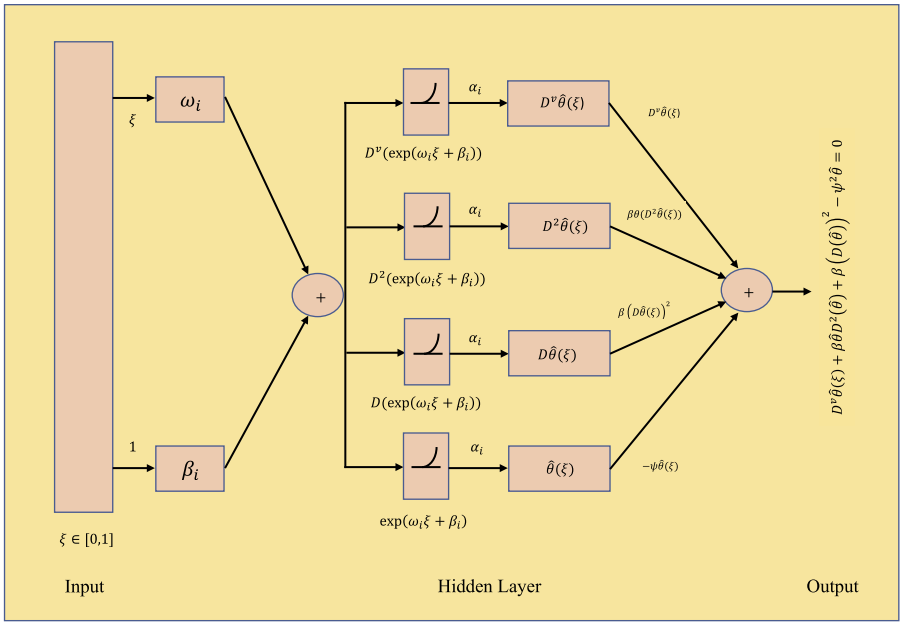

Figure 3 ANN structure for the problem

$$E_2 = \frac{1}{2}\left(\hat{\theta}'(0)^2 + \left(\hat{\theta}(1)-1\right)^2\right). \tag{19}$$

Here, E_1 is related to the differential equation and E_2 is related to the initial and boundary conditions. We try to find the weights α_i, ω_i, and β_i in Eq. (15) such that E_1 and E_2 approach zero, then E will also approach zero. Hence the approximate solution $\hat{\theta}(\xi)$ will approach the exact solution $\theta(\xi)$.

4.2 Cuckoo search

Inspired by the cuckoo bird's breeding behavior, a metaheuristic algorithm was developed which is called the cuckoo search algorithm [59]. The female bird lays eggs in other host birds' nests and they unintentionally raise her brood. When the host bird finds the egg of the cuckoo bird in her nest, it either throws it out of the nest or starts making her own brood elsewhere [60].

In the cuckoo search algorithm, the solution is represented by the egg of the host bird and the new candidate solution is represented by cuckoo's egg. There are three rules that are described for cuckoo search and those are [61]: (1) the cuckoo lays a single egg at a time and puts it in the host's nest; (2) the nests that have a high quality egg, i.e., a better solution will go to the next generation; and (3) there is a fixed number of host nests, and the host bird can find an alien egg with certain probability.

Assuming $\boldsymbol{x}_i = (x_{i1}, x_{i2}, \ldots, x_{iD})$ as the position for the ith egg (solution) then updated solution x_i^{new} is generated by Levy flights as given below:

$$\begin{aligned} x_i^{\text{new}} &= x_i^{\text{old}} + \alpha(x_l - x_g) \oplus \text{Levy}(\beta), \\ &= x_i^{\text{old}} + \frac{0.01u}{|\nu|^{1/\beta}}(x_i - x_g), \end{aligned} \tag{20}$$

where the product $\oplus$ is entry-wise multiplication; the Levy flight exponent is denoted by β; the step size for a cuckoo is determined by a positive parameter α; the best solution within the current population is denoted by x_g; u and v are random numbers:

$$u \sim N\left(0, \sigma_u^2\right), \qquad v \sim N\left(0, \sigma_v^2\right), \tag{21}$$

$$\sigma_u = \left[\frac{\sin(\pi\beta/2) \cdot \Gamma(1+\beta)}{2^{(\beta-1)/2}\beta \cdot \Gamma(\frac{1+\beta}{2})}\right]^{1/\beta}, \qquad \sigma_v = 1, \tag{22}$$

where Γ is used for gamma function, and β controls the value of σ_u. There is a discovery operator in CS which is used to replace the discovered nests with a probability (pa). The equation that is used to update the solution is given as follows:

$$x_{ij}^{\text{new}} = \begin{cases} x_{ij}^{\text{old}} + \text{rand} \cdot (x_{r1,j}(k) - x_{r2j}(k)) & \text{if } P > pa, \\ x_{ij}^{\text{old}}(k) & \text{else}, \end{cases} \tag{23}$$

where ${x_{ij}}^{\text{new}}$ is the jth element of the ith solution ${x_i}^{\text{new}}$; $x_{r1,j}$ and $x_{r2,j}$ are the jth elements of the two solutions x_{r1} and x_{r2}, where $r1$ and $r2$ are two different integers in interval $[1, NP]$, where NP represents size of population, pa represents the discovery probability, P and rand are some random numbers that belong to the interval $[0, 1]$.

4.3 Biogeography-based optimization

Biogeography-based optimization (BBO) is an evolutionary algorithm which is inspired by different characteristics of species living in the islands [62]. In BBO, each habitat is considered as a candidate solution having some habitat's suitability index (HSI), which is employed for measurement of the quality of a habitat. A habitat (solution) is represented by some suitability index variables (SIV). Two types of operators, i.e., migration and mutation, are used in BBO that are employed for the evolution of the population. In migration process, the solutions with high HSI share their characteristics with the solutions having low HSI and the solutions with low HSI accept new characteristics from the solutions with high HSI.

In BBO, population is randomly initialized with NP habitats (solutons). Each generation sorts the population from the best to the worst and immigration and emigration rates λ and μ respectively are assigned to each habitat:

$$\begin{cases} \lambda_i = I(1 - \frac{S_i}{NP}), \\ \mu_i = E\frac{S_i}{NP}, \end{cases} \tag{24}$$

where immigration (I) and emigration (E) rates are such that $I = E = 1$; S_i represents the number of species of the habitats and $S_i = NP - i$. Accordingly, for the best solution the S_i value is $NP - 1$, and for the second best solution the S_i value is $NP - 2$, and for the worst solution the S_i value is 0.

The migration mixes the features within the population that modifies the solutions. After migration, to modify the solutions, BBO also uses the mutation operator.

4.4 Heterogeneous cuckoo search algorithm based on BBO

CS and BBO are hybridized because CS uses the Levy flights to modify the solutions as it is good at exploration, and BBO modifies the solutions using the migration operator as it is good at exploitation. Combining the exploration and exploitation, a hybrid metaheuristic algorithm is developed which is known as BBO-based heterogeneous cuckoo search (BHCS) algorithm. The proposed BHCS algorithm has two main stages that are the heterogeneous cuckoo search and the discovery based on biogeography. The details of these two stages are explained in the next section.

4.4.1 Heterogeneous cuckoo search strategy

At first stage, the BHCS algorithm uses the Levy flights and quantum mechanism based heterogeneous cuckoo search. This strategy is inspired by quantum mechanism and was first presented in [60, 63]. The rules to update the solutions by heterogeneous cuckoo search are given as follows [60, 63]:

$$x_i^{\text{new}} = \begin{cases} x_i^{\text{old}} + \alpha \cdot (x_i - x_g) \oplus \text{Levy}(\beta) & \frac{2}{3} < sr \leq 1 \text{ (a)}, \\ \bar{x} + L \cdot (\bar{x} - x_i^{\text{old}}) & \frac{1}{3} < sr \leq \frac{2}{3} \text{ (b)}, \\ x_i^{\text{old}} + \varepsilon \cdot (x_g - x_i^{\text{old}}) & \text{else (c)}, \end{cases} \tag{25}$$

where $L = \delta \ln(1/\eta)$, $\varepsilon = \delta \exp(\eta)$, x_g is used for the best solution at the current iteration; $\bar{x} = \frac{1}{NP} \sum_{i=1}^{NP} x_i$ represents the mean of all solutions; sr and η are random numbers in the interval $[0, 1]$. Equation (25) shows that heterogeneous cuckoo search employs three equations to update the solutions with the same probabilities. The first equation is related to Levy flights in original cuckoo search and the second and third equations to update the solutions are based on quantum mechanism. Updating the solutions using heterogeneous rules diversifies the search and follows the direction towards the real global region.

4.4.2 Biogeography-based discovery operator

At the second stage, new solutions are generated using a discovery operator. When the host bird finds an alien egg with probability pa, it abandons the old nest and starts making a new nest based on the migration operator.

Initially, solutions are listed from the best to worst, and an immigration rate μ is assigned to each solution:

$$\mu_l = E \frac{S_i}{NP}, \tag{26}$$

where $E = 1$ represents the maximum emigration rate; $S_i = NP - i$ represents the number of species in solutions.

In biogeography-based discovery operator, those solutions having best fitness value share their characteristics with other solutions, which helps to enhance the exploitation.

4.4.3 Overall BHCS algorithm

The BHCS algorithm uses a cascading structure for the implementation of its two steps. The cooperation between heterogeneous search strategy and biogeography-based discovery operator can efficiently balance the exploitation and exploration.

5 Performance metrics

We have performed 100 simulations on all four problems to establish the stability, adaptability, and certainty of the BHCS algorithm. For this purpose, we have determined the mean absolute deviation (MAD) in solutions, root-mean-square error (RMSE), error in Nash–Sutcliffe efficiency (ENSE), Theil's inequality coefficient (TIC), and Nash–Sutcliffe efficiency (NSE). The analytical definition of these indexes are provided in Eqs. (27)–(30),

$$MAD = \frac{1}{N}\sum_{m=1}^{N}|\theta_m - \hat{\theta}_m|, \tag{27}$$

$$TIC = \frac{\sqrt{\frac{1}{N}\sum_{m=1}^{N}(\theta_m - \hat{\theta}_m)^2}}{\left(\sqrt{\frac{1}{N}\sum_{m=1}^{N}\theta_m^2} + \sqrt{\frac{1}{N}\sum_{m=1}^{N}\hat{\theta}_m^2}\right)}, \tag{28}$$

$$NSE = 1 - \frac{\sum_{m=1}^{N}(\theta_m - \hat{\theta}_m)^2}{\sum_{m=1}^{N}(\theta_m - \bar{\theta}_m)^2}, \quad \bar{\theta}_m = \frac{1}{N}\sum_{m=1}^{N}\theta_m, \tag{29}$$

$$ENSE = 1 - NSE. \tag{30}$$

6 Results and discussion

In this paper, the biogeography-based heterogeneous cuckoo search (BHCS) algorithm is used to train the ANN model for the solution of fractional differential equations. We have considered the fractional form of the energy balance equation (6) in order to find the temperature in straight fins. We have considered the cases with integer and fractional orders. The problems are solved using the ANN modeling given in Eqs. (15) and (16). In our ANN network, we have taken 10 neurons with 30 unknown weights α, ω, and β. The training is performed over the interval $[0,1]$ with a step size of 0.1. The domain has 11 grid points.

6.1 Case 1

In the first case, we have taken $\beta = 0$, $\nu = 2$. Using these values, Eq. (6) becomes

$$\frac{d^2\theta}{d\xi^2} - \psi^2\theta = 0; \quad 0 \le \xi \le 1, \tag{31}$$

with boundary conditions

$$\theta'(0) = 0, \qquad \theta(1) = 1. \tag{32}$$

The fitness function for Eqs. (31) and (32) is given as

$$\min \quad E = \frac{1}{11}\sum_{m=0}^{10}\left(\frac{d^2\hat{\theta}}{d\xi^2} - \psi^2\hat{\theta}\right)^2 + \frac{1}{2}\left(\left(\hat{\theta}'(0)\right)^2 + \left(\hat{\theta}(1) - 1\right)^2\right). \tag{33}$$

Equation (33) is minimized for $\psi = 0.2$, $\psi = 0.5$, and $\psi = 0.8$ using the ANN–BHCS algorithm. The minimum fitness values obtained for the cases with $\psi = 0.2$, $\psi = 0.5$, and

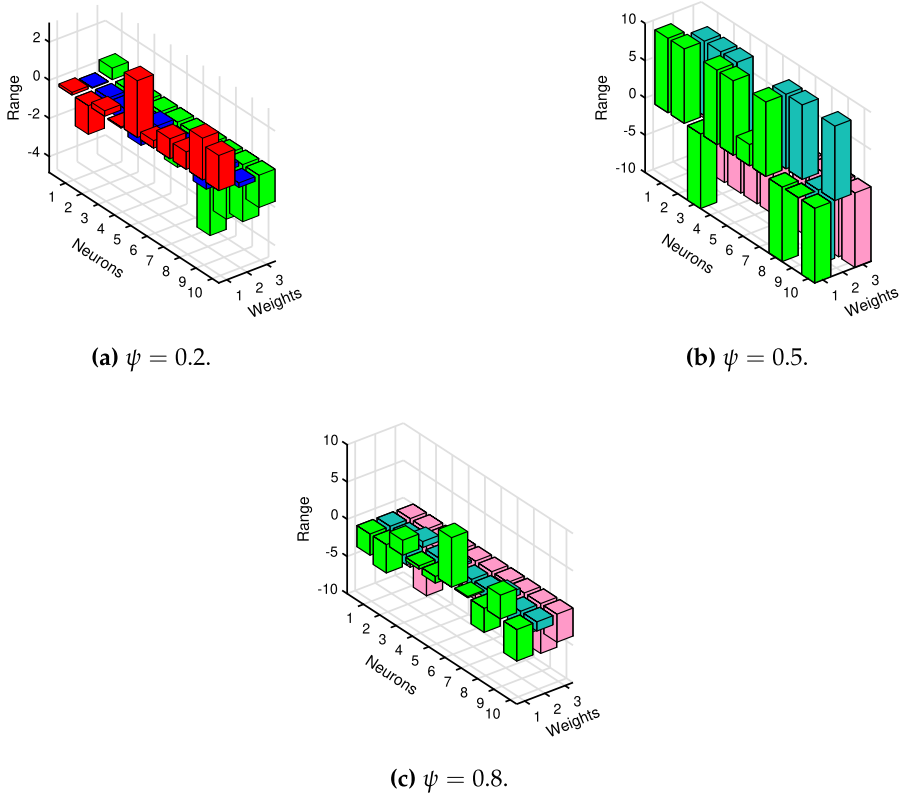

(a) $\psi = 0.2$. **(b)** $\psi = 0.5$. **(c)** $\psi = 0.8$.

Figure 4 Weights obtained by the ANN–BHCS algorithm for case 1

ψ = 0.8 are 7.4829E−13, 1.5272E−16, and 2.8616E−12 respectively. Weights obtained by the ANN–BHCS algorithm for different values of ψ in case 1 are given in Fig. 4.

Using the weights given in Fig. 4, the series solutions for case 1 are given as follows:

Solution for ψ = 0.2:

$$\begin{aligned}\hat{\theta}(\xi) = {} & 0.143377926259098e^{(-0.0418794570500770*\xi+0.603339509800116)} \\ & - 1.50409601849347e^{(-0.581908044758456*\xi-2.01551159960342)} \\ & + 0.287241489951004e^{(-0.671405234875654*\xi-0.731521145322519)} \\ & - 0.0627038559905543e^{(-1.36851490007073*\xi-0.436732558847139)} \\ & + 2.97799690160653e^{(0.208371755956944*\xi-2.36837490446120)} \\ & + 0.394989568829285e^{(-0.586047360504350*\xi-1.99633165510105)} \\ & + 1.04859467368134e^{(0.261805873347917*\xi-4.83414069981780)} \\ & + 0.918091810798712e^{(-1.44365419755033*\xi-3.41866339844307)} \\ & + 2.19401669184716e^{(0.251280939194522*\xi-2.99313408698317)} \\ & + 1.84383655001332e^{(-0.239279689235954*\xi-1.69054475191618)},\end{aligned} \tag{34}$$

Solution for $\psi = 0.5$:

$$\begin{aligned}\hat{\theta}(\xi) = {} & 10e^{(0.499970067232250*\xi-3.11686717118239)} \\ & + 10e^{(10*\xi-10)} - 10e^{(10*\xi-10)} + 10e^{(10*\xi-10)} \\ & + 9.99494624581934e^{(0.527213929554713*\xi-9.99999999999726)} \\ & + 2.86432831656622e^{(-0.500001463874875*\xi-1.86559907908470)} \\ & + 10e^{(9.99999999998309*\xi-10)} - 9.99999999999504e^{(10*\xi-10)} \\ & - 1.54342599995394e-05e^{(-9.98889167939289*\xi-10)} - 10e^{(10*\xi-10)},\end{aligned} \tag{35}$$

Solution for $\psi = 0.8$:

$$\begin{aligned}\hat{\theta}(\xi) = {} & -2.84540527255357e^{(-3.21845338461347*\xi-6.53112157800192)} \\ & - 3.80413421079954e^{(-3.74181618183772*\xi-8.93065320014428)} \\ & + 2.00944346021810e^{(0.799869640284646*\xi-1.62836178434453)} \\ & - 0.441669875127631e^{(-0.981705252103056*\xi-4.67920234633275)} \\ & - 0.900148712340136e^{(0.296185270518098*\xi-5.15015758661538)} \\ & + 6.63668690521927e^{(-0.779416608705294*\xi-2.89499226031466)} \\ & + 0.167565735886103e^{(-1.23922653155550*\xi-0.390700545289821)} \\ & - 3.22533792775341e^{(0.822874709544892*\xi-5.18290223782813)} \\ & + 3.19253397853502e^{(-3.39413566604332*\xi-6.69094305479483)} \\ & - 4.23009948394512e^{(-1.23074833318238*\xi-3.75559355870230)}.\end{aligned} \tag{36}$$

Exact and approximate solutions for $\psi = 0.2$, $\psi = 0.5$, and $\psi = 0.8$ obtained by HPM, VIM, HPSTM, and ANN–BHCS algorithm are given in Tables 1, 2 and 3 respectively. The absolute errors in approximate solutions for $\psi = 0.2$, $\psi = 0.5$, and $\psi = 0.8$ are given in Tables 4, 5 and 6 respectively. The tables show that the absolute errors in solutions obtained by the ANN–BHCS algorithm are less than those of the HPM, VIM, and HPSTM, which shows that the ANN–BHCS algorithm gives better solutions than other techniques. The exact and approximate solutions obtained by the ANN–BHCS algorithm for different values of ψ are also plotted in Fig. 5(a). The figure shows that the solutions obtained by the ANN–BHCS algorithm are very close to the exact solution. From Fig. 5(a), we can see that the dimensionless temperature θ decreases as the value of thermo-geometric fin parameter ψ increases. The absolute errors in solutions for different values of ψ are plotted in Fig. 5(b). The absolute errors in solutions for $\psi = 0.2$, $\psi = 0.5$, and $\psi = 0.8$ are in the range 2.25E–08 to 7.71E–09, 4.19E–09 to 8.80E–09, and 2.34E–07 to 4.25E–07 respectively. Convergence of the fitness values for different values of ψ is given in Fig. 5(c). Histogram plots of the values of performance metrics are given in Figs. 6 and 7. In Fig. 6, the histograms for MAD and TIC values are given, which shows that more than 90% of the values are very close to zero. Figure 7 shows that more than 90% of the fitness and ENSE values are very close to zero, which shows the accuracy of the ANN–BHCS algorithm.

Table 1 Exact and approximate solutions for case 1 with $\psi = 0.2$

ξ	Exact	HPM [6]	VIM [52]	HPSTM [21]	ANN–BHCS
0	0.980327998	0.9803	0.9803	0.980328	**0.980328074**
0.1	0.980524070	0.9805	0.9805	0.980524	**0.980524147**
0.2	0.981112365	0.9805	0.9811	0.981112	**0.981112432**
0.3	0.982093117	0.9821	0.9820	0.982093	**0.982093168**
0.4	0.983466721	0.9835	0.9834	0.983467	**0.983466756**
0.5	0.985233724	0.9852	0.9852	0.985234	**0.985233752**
0.6	0.987394833	0.9874	0.9873	0.987395	**0.987394863**
0.7	0.989950914	0.9900	0.9899	0.989951	**0.989950948**
0.8	0.992902988	0.9929	0.9929	0.992903	**0.992903022**
0.9	0.996252237	0.9963	0.9962	0.996252	**0.996252260**
1	1.000000000	1.0000	1.0000	1.000000	**1.000000005**

Table 2 Exact and approximate solutions for case 1 with $\psi = 0.5$

ξ	Exact	HPM [6]	VIM [52]	HPSTM [21]	ANN–BHCS
0	0.886818884	0.8868	0.8868	0.886833	**0.886818875**
0.1	0.887927639	0.8879	0.8879	0.887942	**0.887927630**
0.2	0.891256675	0.8913	0.8912	0.891271	**0.891256667**
0.3	0.896814317	0.8968	0.8968	0.896829	**0.896814309**
0.4	0.904614462	0.9046	0.9046	0.904629	**0.904614455**
0.5	0.914676614	0.9147	0.9146	0.914691	**0.914676608**
0.6	0.927025934	0.9270	0.9270	0.92704	**0.927025929**
0.7	0.941693302	0.9417	0.9416	0.941707	**0.941693297**
0.8	0.958715394	0.9587	0.9587	0.958727	**0.958715390**
0.9	0.978134774	0.9781	0.9781	0.978142	**0.978134769**
1	1.000000000	1.0000	1.0000	1.000000	**0.999999996**

Table 3 Exact and approximate solutions for case 1 with $\psi = 0.8$

ξ	Exact	HPM [6]	VIM [52]	HPSTM [21]	ANN–BHCS
0	0.747699918	0.7477	0.7477	0.747893	**0.747699494**
0.1	0.750093834	0.7501	0.7500	0.750288	**0.750093436**
0.2	0.757290912	0.7573	0.7572	0.757487	**0.757290522**
0.3	0.769337237	0.7693	0.7693	0.769536	**0.769336857**
0.4	0.786309946	0.7863	0.7863	0.786512	**0.786309593**
0.5	0.808317724	0.8083	0.8083	0.808523	**0.808317413**
0.6	0.835501495	0.8355	0.8355	0.835705	**0.835501227**
0.7	0.868035328	0.8680	0.8680	0.868229	**0.868035088**
0.8	0.906127550	0.9061	0.9061	0.906294	**0.906127316**
0.9	0.950022083	0.9500	0.9500	0.950131	**0.950021836**
1	1.000000000	1.0000	1.0000	1.000000	**0.999999740**

Table 4 Absolute errors in solutions for case 1 with $\psi = 0.2$

ξ	HPM [6]	VIM [52]	HPSTM [21]	ANN–BHCS
0	2.80E–05	2.80E–05	2.36E–09	**7.68E–08**
0.1	2.41E–05	2.41E–05	6.98E–08	**7.71E–08**
0.2	0.00061	1.24E–05	3.65E–07	**6.76E–08**
0.3	6.88E–06	9.31E–05	1.17E–07	**5.06E–08**
0.4	3.33E–05	6.67E–05	2.79E–07	**3.51E–08**
0.5	3.37E–05	3.37E–05	2.76E–07	**2.79E–08**
0.6	5.17E–06	9.48E–05	1.67E–07	**2.95E–08**
0.7	4.91E–05	5.09E–05	8.59E–08	**3.41E–08**
0.8	2.99E–06	2.99E–06	1.16E–08	**3.36E–08**
0.9	4.78E–05	5.22E–05	2.37E–07	**2.25E–08**
1	0.000000	0.000000	**0.000000**	4.68E–09

Table 5 Absolute errors in solutions for case 1 with $\psi = 0.5$

t	HPM [6]	VIM [52]	HPSTM [21]	ANN–BHCS
0	1.89E–05	1.89E–05	1.41E–05	**8.80E–09**
0.1	2.76E–05	2.76E–05	1.44E–05	**8.57E–09**
0.2	4.33E–05	5.67E–05	1.43E–05	**8.12E–09**
0.3	1.43E–05	1.43E–05	1.47E–05	**7.50E–09**
0.4	1.45E–05	1.45E–05	1.45E–05	**6.80E–09**
0.5	2.34E–05	7.66E–05	1.44E–05	**6.12E–09**
0.6	2.59E–05	2.59E–05	1.41E–05	**5.54E–09**
0.7	6.70E–06	9.33E–05	1.37E–05	**5.08E–09**
0.8	1.54E–05	1.54E–05	1.16E–05	**4.74E–09**
0.9	3.48E–05	3.48E–05	7.23E–06	**4.47E–09**
1	0.000000	0.000000	0.000000	**4.19E–09**

Table 6 Absolute errors in solutions for case 1 with $\psi = 0.8$

ξ	HPM [6]	VIM [52]	HPSTM [21]	ANN–BHCS
0	8.18E–08	8.18E–08	1.93E–04	**4.25E–07**
0.1	6.17E–06	9.38E–05	1.94E–04	**3.98E–07**
0.2	9.09E–06	9.09E–05	1.96E–04	**3.90E–07**
0.3	3.72E–05	3.72E–05	1.99E–04	**3.80E–07**
0.4	9.95E–06	9.95E–06	2.02E–04	**3.53E–07**
0.5	1.77E–05	1.77E–05	2.05E–04	**3.11E–07**
0.6	1.49E–06	1.49E–06	2.04E–04	**2.68E–07**
0.7	3.53E–05	3.53E–05	1.94E–04	**2.40E–07**
0.8	2.76E–05	2.76E–05	1.66E–04	**2.34E–07**
0.9	2.21E–05	2.21E–05	1.09E–04	**2.47E–07**
1	0.000000	0.000000	0.000000	**2.60E–07**

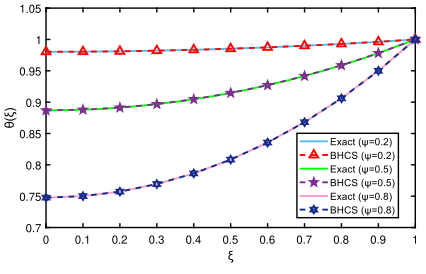

(a) Solutions for case 1.

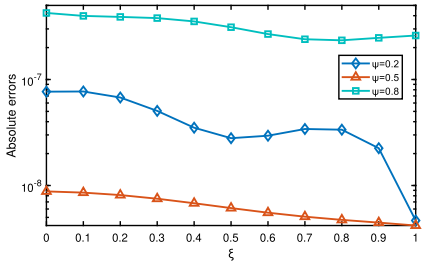

(b) Absolute errors for case 1.

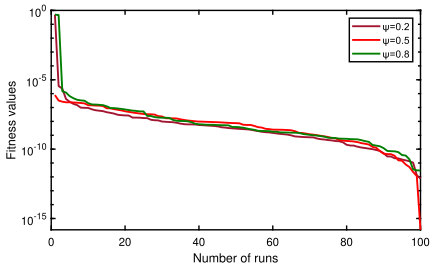

(c) Convergence of the fitness values for case 1.

Figure 5 Results obtained by the ANN–BHCS algorithm for case 1

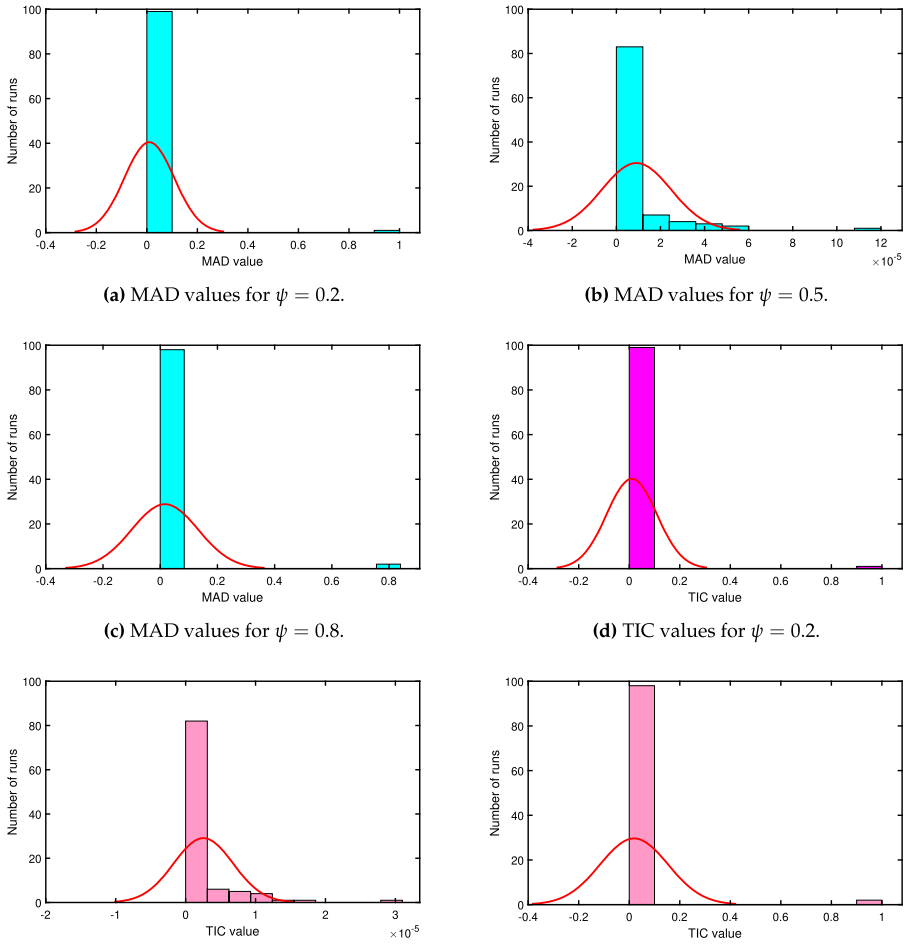

(a) MAD values for $\psi = 0.2$.

(b) MAD values for $\psi = 0.5$.

(c) MAD values for $\psi = 0.8$.

(d) TIC values for $\psi = 0.2$.

(e) TIC values for $\psi = 0.5$.

(f) TIC values for $\psi = 0.8$.

Figure 6 Histograms of MAD and TIC for case 1

6.2 Case 2

In the second case, we have taken $\psi = 0.5$ and $\nu = 2$. Using these values, Eq. (6) becomes

$$\frac{d^2\theta}{d\xi^2} + \beta\theta\frac{d^2\theta}{d\xi^2} + \beta\left(\frac{d\theta}{d\xi}\right)^2 - (0.5)^2\theta = 0; \quad 0 \le \xi \le 1, \tag{37}$$

with boundary conditions

$$\theta'(0) = 0, \qquad \theta(1) = 1. \tag{38}$$

The fitness function for Eqs. (37) and (38) is given as

$$\begin{aligned} \min \quad E = {} & \frac{1}{11}\sum_{m=0}^{10}\left(\frac{d^2\hat{\theta}}{d\xi^2} + \beta\hat{\theta}\frac{d^2\hat{\theta}}{d\xi^2} + \beta\left(\frac{d\hat{\theta}}{d\xi}\right)^2 - (0.5)^2\hat{\theta}\right)^2 \\ & + \frac{1}{2}\left(\left(\hat{\theta}'(0)\right)^2 + \left(\hat{\theta}(1) - 1\right)^2\right). \end{aligned} \tag{39}$$

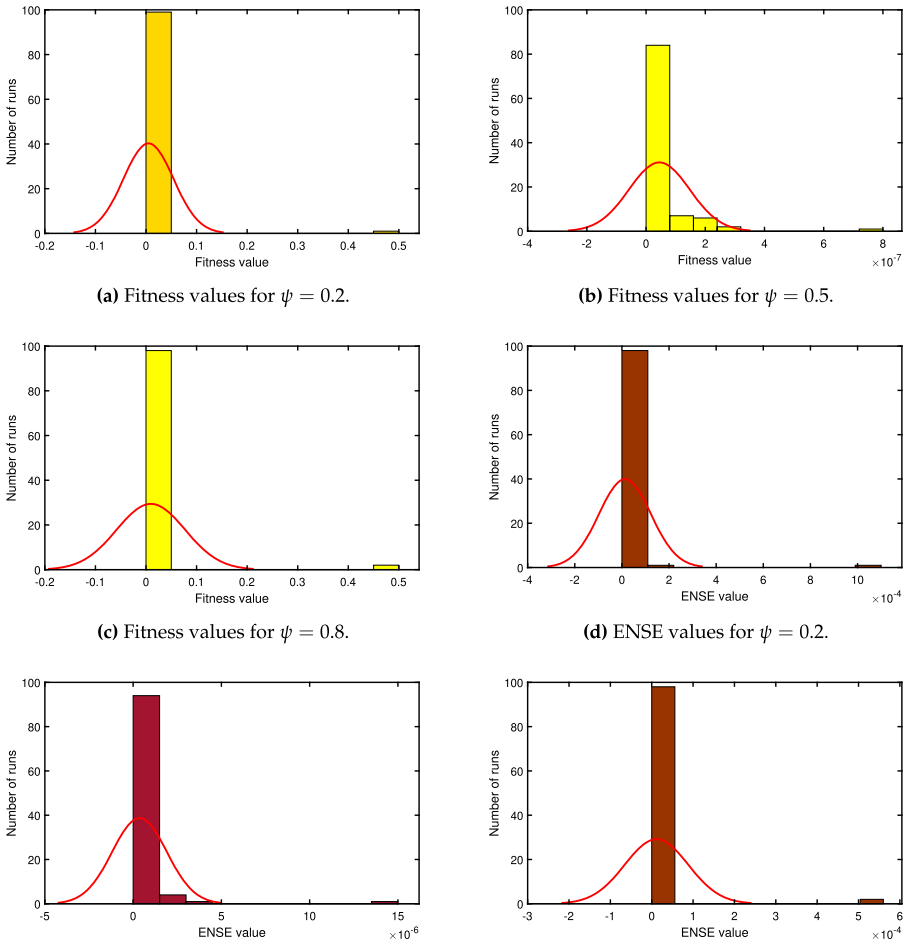

(a) Fitness values for $\psi = 0.2$.

(b) Fitness values for $\psi = 0.5$.

(c) Fitness values for $\psi = 0.8$.

(d) ENSE values for $\psi = 0.2$.

(e) ENSE values for $\psi = 0.5$.

(f) ENSE values for $\psi = 0.8$.

Figure 7 Histograms of ENSE and fitness values for case 1

Equation (39) is minimized for different values of β using the ANN–BHCS algorithm. A total of 100 simulations were performed for different values of β. The minimum fitness values for $\beta = -0.5, -0.3, -0.1, 0.1, 0.3$, and 0.5 are 7.6027E−10, 2.8034E−11, 6.4330E−12, 1.3345E−10, 2.8926E−12, and 3.7965E−12 respectively. Weights obtained to minimize the fitness function for different values of β are plotted in Fig. 8. Using the weights given in Fig. 8, series solutions of case 2 for different values of β are given as follows:

Solution for $\beta = -0.5$:

$$\hat{\theta}(\xi) = 1.3350e^{(-0.7910*\xi-0.6658)} + \cdots + 0.96921e^{(-3.0480*\xi-2.5067)}, \tag{40}$$

Solution for $\beta = -0.3$:

$$\hat{\theta}(\xi) = 0.8911e^{(3.2514*\xi-9.0745)} + \cdots - 2.8323e^{(1.5411*\xi-9.8469)}, \tag{41}$$

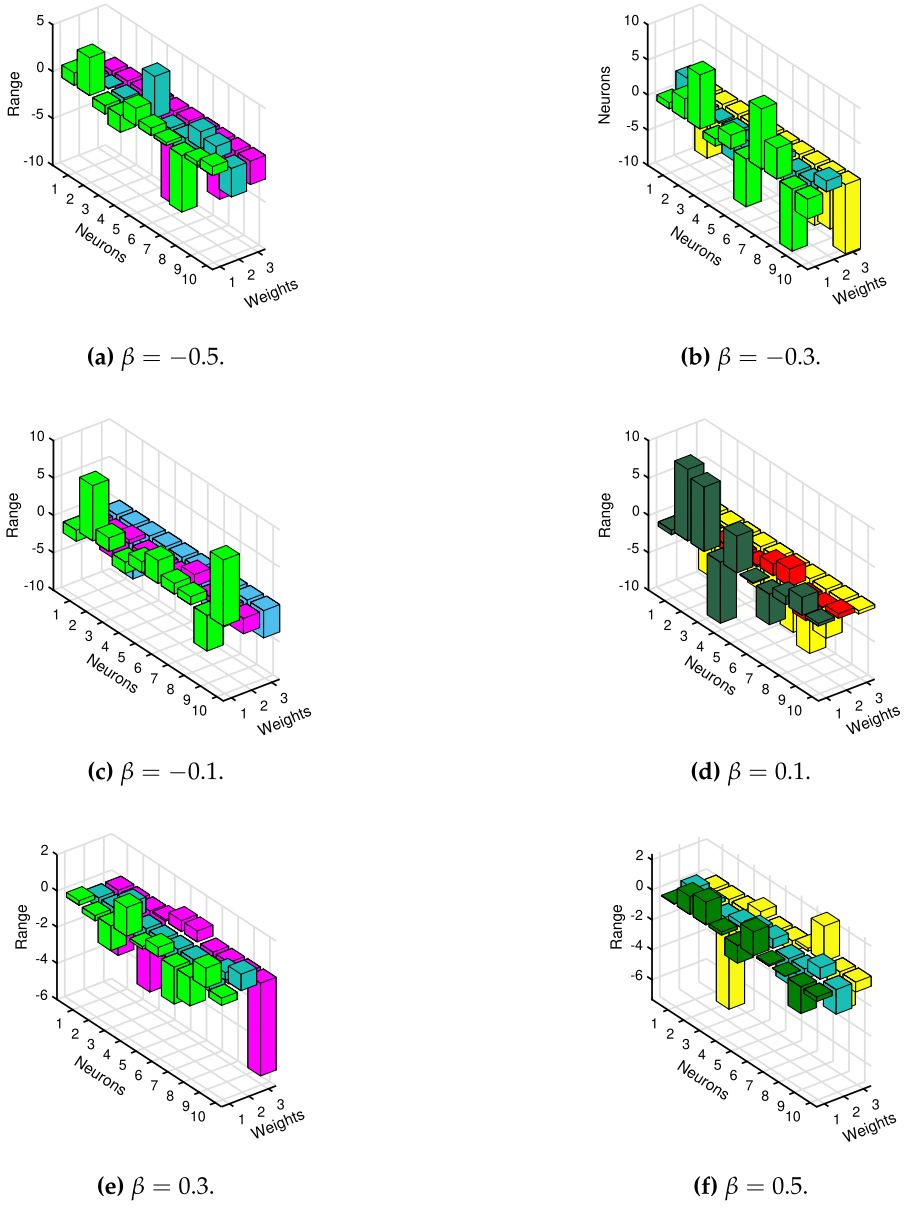

(a) $\beta = -0.5$. **(b)** $\beta = -0.3$.

(c) $\beta = -0.1$. **(d)** $\beta = 0.1$.

(e) $\beta = 0.3$. **(f)** $\beta = 0.5$.

Figure 8 Weights obtained by ANN–BHCS algorithm for case 2

Solution for $\beta = -0.1$:

$$\hat{\theta}(\xi) = -1.4834e^{(-1.9619*\xi-1.9046)} + \cdots + 8.8526e^{(-2.0635*\xi-3.6484)}, \tag{42}$$

Solution for $\beta = 0.1$:

$$\hat{\theta}(\xi) = -0.6059e^{(-0.8974*\xi-8.3929)} + \cdots + 0.3641e^{(0.6138*\xi-0.4443)}, \tag{43}$$

Solution for $\beta = 0.3$:

$$\hat{\theta}(\xi) = 0.2523e^{(-0.5144*x-3.6000)} + \cdots - 0.4030e^{(0.9104*x-5.1234)}, \tag{44}$$

Table 7 Solutions of case 2 for different values of β

ξ	$\beta = -0.5$	$\beta = -0.3$	$\beta = -0.1$	$\beta = 0.1$	$\beta = 0.3$	$\beta = 0.5$
0	0.80870903	0.84895272	0.87632760	0.89575861	0.91012117	0.92110851
0.1	0.81040774	0.85037735	0.87752844	0.89678637	0.91101487	0.92189683
0.2	0.81552617	0.85466099	0.88113548	0.89987138	0.91369658	0.92426187
0.3	0.82413110	0.86183292	0.88716148	0.90501908	0.91816818	0.92820385
0.4	0.83633707	0.87194260	0.89562778	0.91223846	0.92443280	0.93372316
0.5	0.85231206	0.88506085	0.90656446	0.92154190	0.93249480	0.94082028
0.6	0.87228676	0.90128139	0.92001057	0.93294525	0.94235971	0.94949584
0.7	0.89656852	0.92072293	0.93601440	0.94646792	0.95403426	0.95975061
0.8	0.92556226	0.94353191	0.95463379	0.96213294	0.96752632	0.97158552
0.9	0.95980197	0.96988620	0.97593654	0.97996694	0.98284490	0.98500159
1	0.99999869	1.00000001	1.00000088	0.99999999	1.00000009	1.00000000

Solution for $\beta = 0.5$:

$$\hat{\theta}(\xi) = 0.0511e^{(0.5214*\xi-1.8989)} + \cdots - 0.3029e^{(-1.6382*\xi-0.6656)}. \tag{45}$$

Numerical solutions for case 2 with different values of thermal conductivity β are given in Table 7. Solutions are also plotted in Fig. 9(a). In this case, the thermo-geometric fin parameter is taken as $\psi = 0.5$ and the thermal conductivity β is varied from −0.5 to 0.5 with a step size of 0.2. From Table 7 and Fig. 9(a), we see that the dimensionless temperature θ increases with increase in the value of β. The accuracy of the ANN–BHCS algorithm can be seen from convergence of the fitness values and histograms of fitness values in Fig. 9.

6.3 Case 3

In the third case, we have taken $\nu = 2$, $\psi = 1.5$, and β is varied from −0.5 to 0.5 with step size 0.2. For this case, Eq. (6) takes the form

$$\frac{d^2\theta}{d\xi^2} + \beta\theta\frac{d^2\theta}{d\xi^2} + \beta\left(\frac{d\theta}{d\xi}\right)^2 - (1.5)^2\theta = 0; \quad 0 \le \xi \le 1, \tag{46}$$

with boundary conditions

$$\theta'(0) = 0, \qquad \theta(1) = 1. \tag{47}$$

The fitness function for Eqs. (46) and (47) is given as

$$\begin{aligned} \min \quad E = {} & \frac{1}{11}\sum_{m=0}^{10}\left(\frac{d^2\hat{\theta}}{d\xi^2} + \beta\hat{\theta}\frac{d^2\hat{\theta}}{d\xi^2} + \beta\left(\frac{d\hat{\theta}}{d\xi}\right)^2 - (1.5)^2\hat{\theta}\right)^2 \\ & + \frac{1}{2}\left(\left(\hat{\theta}'(0)\right)^2 + \left(\hat{\theta}(1) - 1\right)^2\right). \end{aligned} \tag{48}$$

The ANN–BHCS algorithm is used to minimize the fitness function for different values of β. The minimum fitness values obtained by the ANN–BHCS algorithm for β = −0.5, −0.3, −0.1, 0.1, 0.3, and 0.5 are 2.5336E−07, 8.0939E−09, 3.0616E−10, 3.6515E−11, 4.3335E−10, and 3.9055E−09 respectively. Weights obtained to minimize the fitness function for different problems are plotted in Fig. 10. Using these weights, the series solutions of different values of β are given as follows:

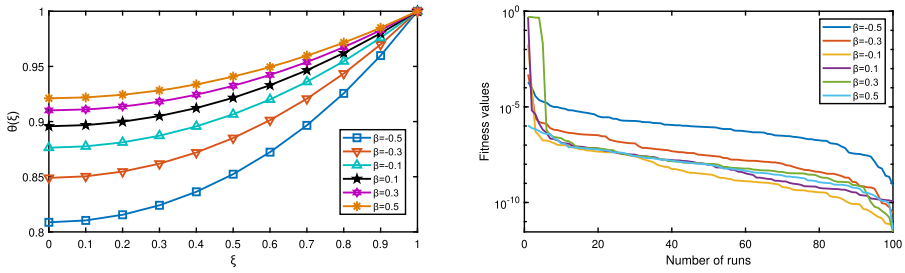

(a) Solutions for case 2. **(b)** Convergence of fitness values for case 2.

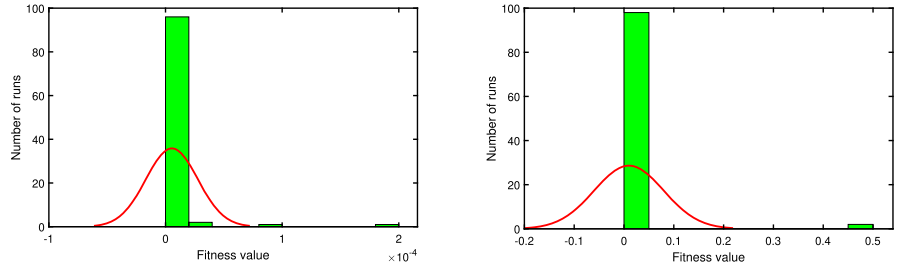

(c) $\beta = -0.5$. **(d)** $\beta = -0.3$.

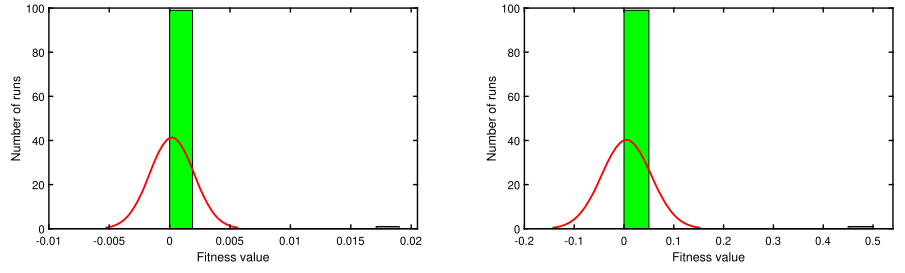

(e) $\beta = -0.1$. **(f)** $\beta = 0.1$.

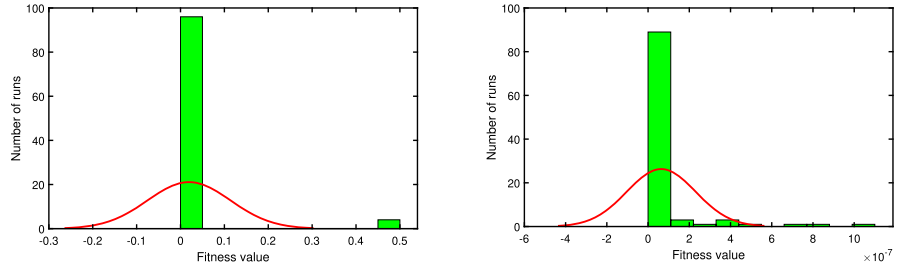

(g) $\beta = 0.3$. **(h)** $\beta = 0.5$.

Figure 9 Results obtained by ANN–BHCS algorithm for case 2

Solution for $\beta = -0.5$:

$$\hat{\theta}(\xi) = 0.3204e^{(0.3247*\xi+0.3378)} + \cdots + 0.6760e^{(0.8112*\xi+0.9999)}, \tag{49}$$

Solution for $\beta = -0.3$:

$$\hat{\theta}(\xi) = 1.8800e^{(-1.3968*\xi-2.0628)} + \cdots + 8.9815e^{(10.0578*\xi-17.6447)}, \tag{50}$$

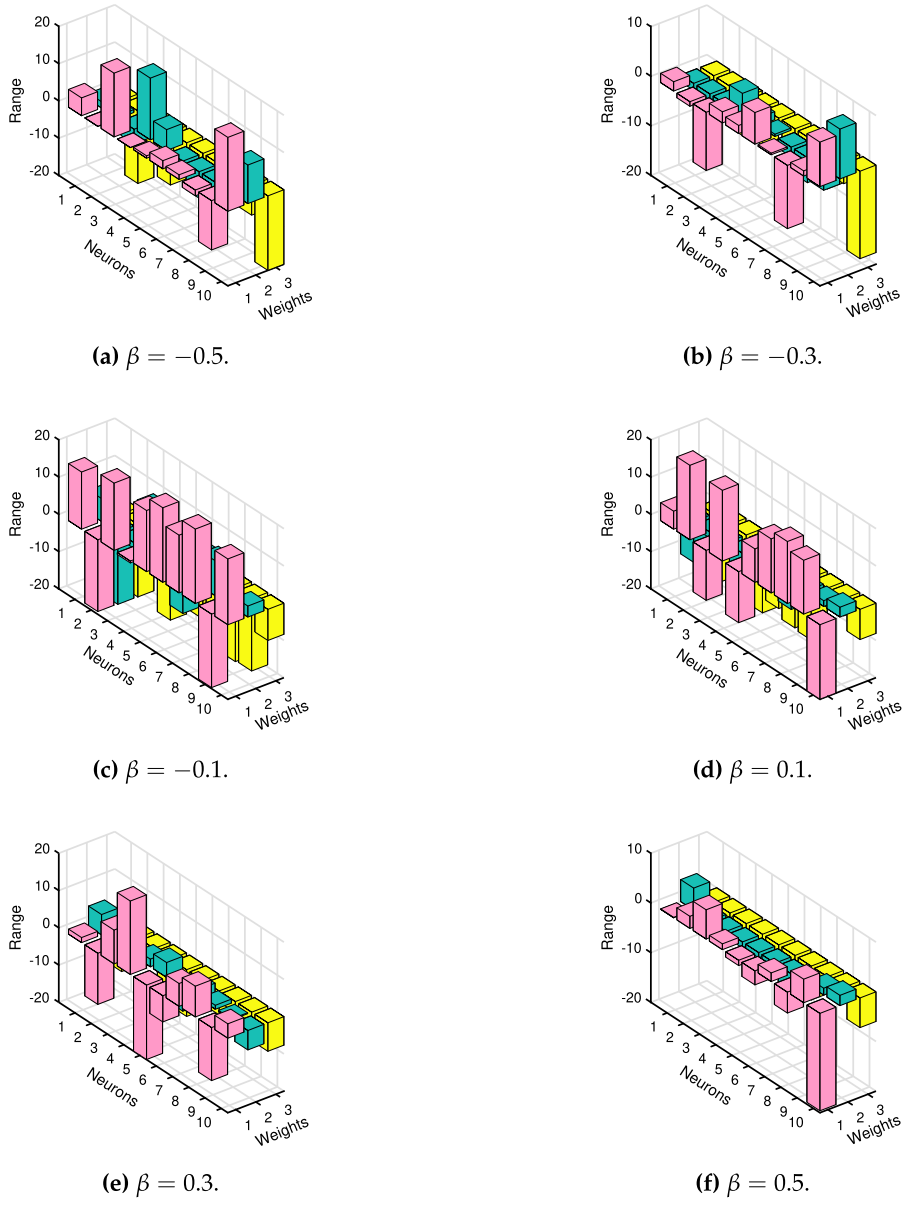

(a) $\beta = -0.5$. **(b)** $\beta = -0.3$.

(c) $\beta = -0.1$. **(d)** $\beta = 0.1$.

(e) $\beta = 0.3$. **(f)** $\beta = 0.5$.

Figure 10 Weights obtained by ANN–BHCS algorithm for case 3

Solution for $\beta = -0.1$:

$$\hat{\theta}(\xi) = 15.3357e^{(6.1567*\xi-19.5578)} + \cdots + 17.6613e^{(2.9498*\xi-8.3558)}, \tag{51}$$

Solution for $\beta = 0.1$:

$$\hat{\theta}(\xi) = 4.8310e^{(-10.9679*\xi-19.0044)} + \cdots - 19.9914e^{(2.6348*\xi-8.1145)}, \tag{52}$$

Solution for $\beta = 0.3$:

$$\hat{\theta}(\xi) = 1.3616e^{(5.4673*\xi-11.9129)} + \cdots + 3.8582e^{(-5.2181*\xi-7.6499)}, \tag{53}$$

Table 8 Solutions of case 3 for different values of β

ξ	$\beta = -0.5$	$\beta = -0.3$	$\beta = -0.1$	$\beta = 0.1$	$\beta = 0.3$	$\beta = 0.5$
0	0.3204530	0.3634227	0.4050497	0.4445395	0.4814116	0.5154265
0.1	0.3247589	0.3680258	0.4098092	0.4493352	0.4861487	0.5200393
0.2	0.3378566	0.3819946	0.4242141	0.4638123	0.5004178	0.5339093
0.3	0.3603275	0.4058207	0.4486484	0.4882419	0.5243908	0.5571308
0.4	0.3932029	0.4403662	0.4837684	0.5230779	0.5583513	0.5898562
0.5	0.4380835	0.4869343	0.5305288	0.5689602	0.6026885	0.6322901
0.6	0.4973826	0.5473863	0.5902239	0.6267186	0.6578902	0.6846835
0.7	0.5747799	0.6243306	0.6645440	0.6973773	0.7245342	0.7473254
0.8	0.6760973	0.7214393	0.7556551	0.7821595	0.8032767	0.8205334
0.9	0.8112633	0.8440041	0.8663089	0.8824905	0.8948398	0.9046434
1	0.9999998	0.9999871	0.9999994	1.0000001	0.9999966	0.9999994

Solution for $\beta = 0.5$:

$$\hat{\theta}(\xi) = 0.0896e^{(4.4270*\xi-7.1525)} + \cdots - 19.6139e^{(2.0733*\xi-5.9705)}. \tag{54}$$

Numerical solutions of case 3 for different values of β are given in Table 8 and Fig. 11(a). Convergence and histogram plots of fitness values are given in Fig. 11. For all the values of β considered in case 3, most of the fitness values are very close to zero, which shows the accuracy of the ANN–BHCS algorithm. From Fig. 11(a), it is clear that the dimensionless temperature θ increases as the values of thermal conductivity β increase.

6.4 Case 4

In this case, we have taken $\nu = 1.75$, $\psi = 0.5$, and β is varied from –0.5 to 0.5 with step size of 0.2. Using these values, Eq. (6) becomes

$$\frac{d^{1.75}\theta}{d\xi^{1.75}} + \beta\theta\frac{d^2\theta}{d\xi^2} + \beta\left(\frac{d\theta}{d\xi}\right)^2 - (0.5)^2\theta = 0; \quad 0 \le \xi \le 1, \tag{55}$$

with boundary conditions

$$\theta'(0) = 0, \qquad \theta(1) = 1. \tag{56}$$

The fitness function for Eqs. (55) and (56) is given by

$$\begin{aligned} \min \quad E = {} & \frac{1}{11}\sum_{m=0}^{10}\left(\frac{d^{1.75}\hat{\theta}}{d\xi^{1.75}} + \beta\hat{\theta}\frac{d^2\hat{\theta}}{d\xi^2} + \beta\left(\frac{d\hat{\theta}}{d\xi}\right)^2 - (0.5)^2\hat{\theta}\right)^2 \\ & + \frac{1}{2}\left(\left(\hat{\theta}'(0)\right)^2 + \left(\hat{\theta}(1) - 1\right)^2\right). \end{aligned} \tag{57}$$

The ANN–BHCS algorithm is used to minimize the fitness function (57) for different values of thermal conductivity β. The minimum of fitness values for $\beta = -0.5, -0.3, -0.1, 0.1$, 0.3, and 0.5 are 6.4804E–08, 2.7340E–09, 2.3225E–10, 7.0940E–10,5.1839E–11, and 4.8342E–11 respectively. Weights obtained by the ANN–BHCS algorithm to minimize fitness functions for different values of β are given in Fig. 12. Using these weights, the series solutions for different values of β are given as follows:

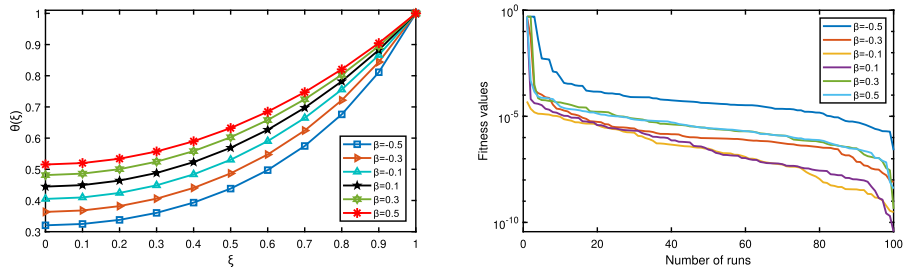

(a) Solutions for case 3. **(b)** Convergence of fitness values for case 3.

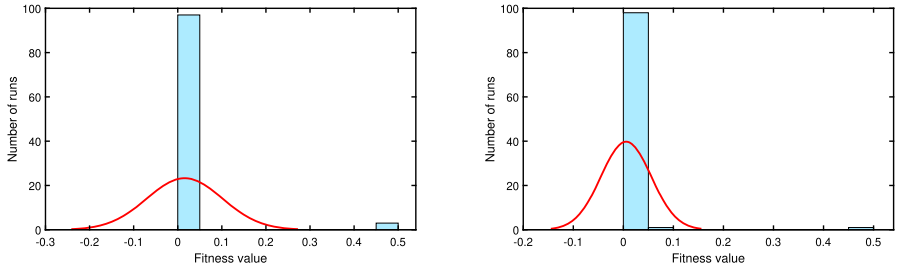

(c) $\beta = -0.5$. **(d)** $\beta = -0.3$.

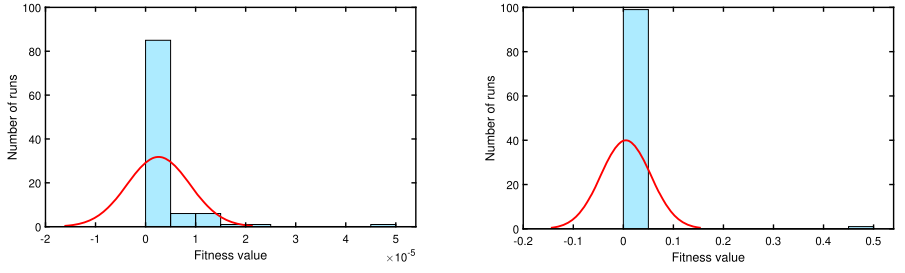

(e) $\beta = -0.1$. **(f)** $\beta = 0.1$.

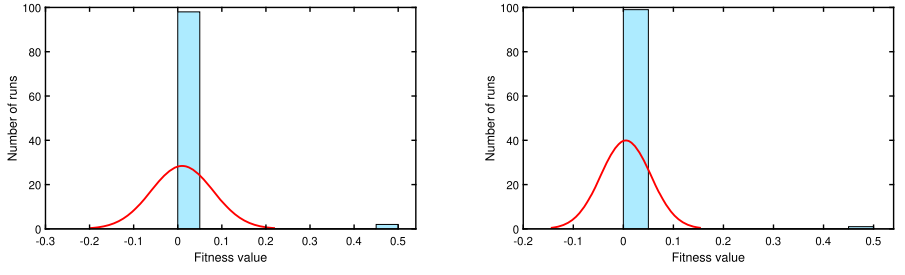

(g) $\beta = 0.3$. **(h)** $\beta = 0.5$.

Figure 11 Results obtained by ANN–BHCS algorithm for case 3

Solution for $\beta = -0.5$:

$$\hat{\theta}(\xi) = 8.1511e^{(0.6314*\xi-2.8504)} + \cdots - 10.5854e^{(2.2229*\xi-8.0687)}, \tag{58}$$

Solution for $\beta = -0.3$:

$$\hat{\theta}(\xi) = 0.0851e^{(-3.5320*\xi-1.5651)} + \cdots - 3.3255e^{(0.2556*\xi-6.5176)}, \tag{59}$$

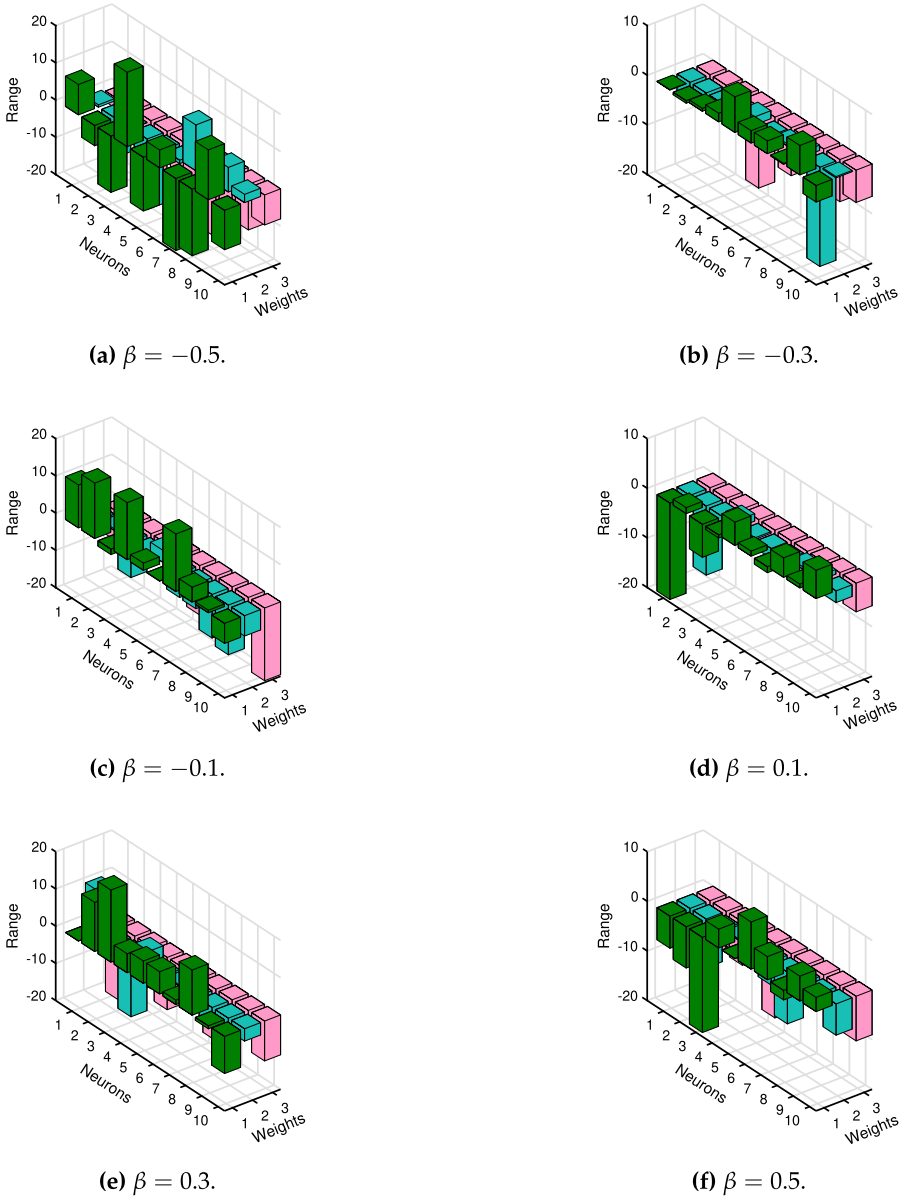

(a) $\beta = -0.5$. **(b)** $\beta = -0.3$.

(c) $\beta = -0.1$. **(d)** $\beta = 0.1$.

(e) $\beta = 0.3$. **(f)** $\beta = 0.5$.

Figure 12 Weights obtained by ANN–BHCS algorithm for case 4

Solution for $\beta = -0.1$:

$$\hat{\theta}(\xi) = 11.5319e^{(-0.5860*\xi-8.0212)} + \cdots - 5.3904e^{(-5.4688*\xi-19.5416)}, \tag{60}$$

Solution for $\beta = 0.1$:

$$\hat{\theta}(\xi) = -19.4309e^{(-2.3198*\xi-11.2920)} + \cdots + 5.6906e^{(-2.3634*\xi-5.7827)}, \tag{61}$$

Solution for $\beta = 0.3$:

$$\hat{\theta}(\xi) = -0.0232e^{(11.2897*\xi-19.9726)} + \cdots - 9.9720e^{(-3.3227*\xi-10.7209)}, \tag{62}$$

Table 9 Solutions of case 4 for different values of β

ξ	$\beta = -0.5$	$\beta = -0.3$	$\beta = -0.1$	$\beta = 0.1$	$\beta = 0.3$	$\beta = 0.5$
0	0.736887254	0.806825310	0.848030903	0.875702486	0.895173165	0.909706168
0.1	0.741421678	0.810242428	0.850464066	0.877525349	0.896627875	0.910894740
0.2	0.751559979	0.818315761	0.856609705	0.882338479	0.900551784	0.914173081
0.3	0.765778410	0.829904509	0.865717768	0.889653279	0.906610595	0.919303417
0.4	0.783893924	0.844693326	0.877505968	0.899249977	0.914639594	0.926159469
0.5	0.805997118	0.862569203	0.891830921	0.911001759	0.924534722	0.934657335
0.6	0.832371069	0.883516938	0.908614294	0.924825732	0.936222607	0.944734751
0.7	0.863600197	0.907592060	0.927819373	0.940666356	0.949649070	0.956343213
0.8	0.900759091	0.934909492	0.949438994	0.958487721	0.964773339	0.969443872
0.9	0.945572821	0.965638253	0.973488179	0.978268589	0.981564669	0.984004942
1	0.999999736	0.999999984	1.000000016	0.999998561	0.999999999	0.999999998

Solution for $\beta = 0.5$:

$$\hat{\theta}(\xi) = -6.4741e^{(-11.6490*\xi-10.8501)} + \cdots + 2.8678e^{(-6.3008*\xi-8.9989)}. \tag{63}$$

Numerical solutions of case 4 for different values of β are given in Table 9 and Fig. 13(a). From Fig. 13(a), it is clear that the dimensionless temperature θ increases as the value of thermal conductivity β goes from −0.5 to 0.5. Convergence of the fitness values for case 4 is given in Fig. 13(b). Histograms of the fitness values for different values of β are given in Figs. 13(c)–13(h). The figures show that more than 90% of the fitness values are very close to zero, which shows the efficiency of the ANN–BHCS algorithm.

6.5 Case 5

In this case, we have taken $\nu = 1.75$, $\psi = 1.5$, and β is varied from −0.5 to 0.5 with step size of 0.2. Using these values, Eq. (6) becomes

$$\frac{d^{1.75}\theta}{d\xi^{1.75}} + \beta\theta\frac{d^2\theta}{d\xi^2} + \beta\left(\frac{d\theta}{d\xi}\right)^2 - (1.5)^2\theta = 0; \quad 0 \le \xi \le 1, \tag{64}$$

with boundary conditions

$$\theta'(0) = 0, \qquad \theta(1) = 1. \tag{65}$$

The fitness function for Eqs. (64) and (65) is given by

$$\begin{aligned} \min \quad E = {} & \frac{1}{11}\sum_{m=0}^{10}\left(\frac{d^{1.75}\hat{\theta}}{d\xi^{1.75}} + \beta\hat{\theta}\frac{d^2\hat{\theta}}{d\xi^2} + \beta\left(\frac{d\hat{\theta}}{d\xi}\right)^2 - (1.5)^2\hat{\theta}\right)^2 \\ & + \frac{1}{2}\left(\left(\hat{\theta}'(0)\right)^2 + \left(\hat{\theta}(1) - 1\right)^2\right). \end{aligned} \tag{66}$$

The ANN–BHCS algorithm is used to minimize the fitness function (66) for different values of β. The minimum fitness values for $\beta = -0.5, -0.3, -0.1, 0.1, 0.3$, and 0.5 are 5.5365E−05, 1.1040E−07, 3.6501E−09, 4.5598E−08, 1.9501E−08, and 9.3420E−09 respectively. Weights obtained to minimize the fitness function for different values of β are given in Fig. 14. Series solutions of case 5 with different values of β are given as follows:

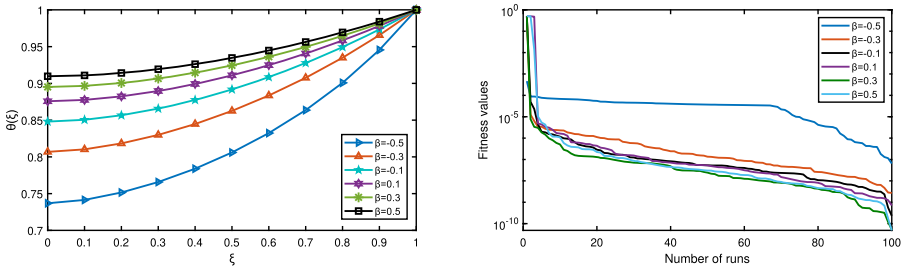

(a) Solutions for case 4.

(b) Convergence of fitness values for case 4.

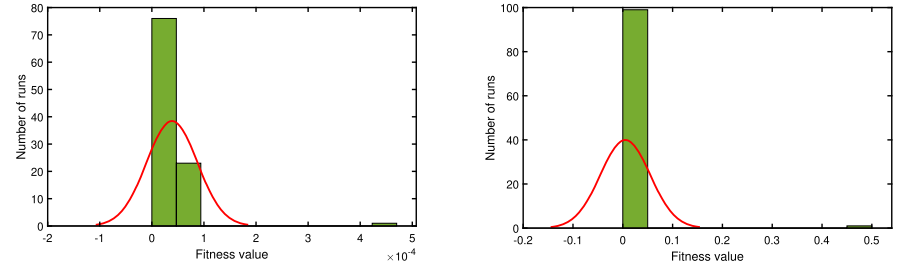

(c) $\beta = -0.5$.

(d) $\beta = -0.3$.

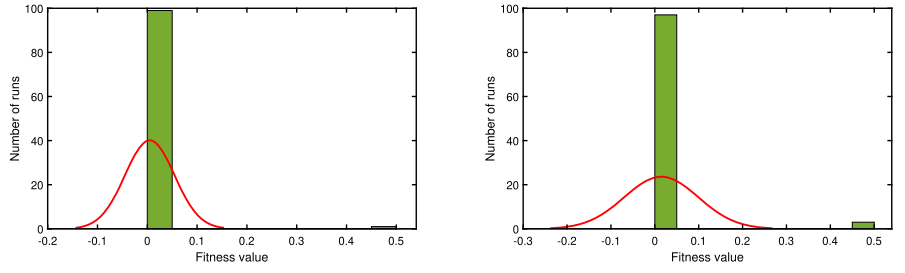

(e) $\beta = -0.1$.

(f) $\beta = 0.1$.

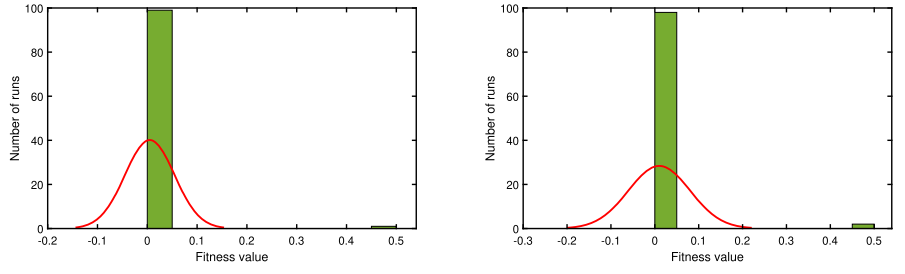

(g) $\beta = 0.3$.

(h) $\beta = 0.5$.

Figure 13 Results obtained by ANN–BHCS algorithm for case 4

Solution for $\beta = -0.5$:

$$\hat{\theta}(\xi) = -19.8513e^{(-18.7508*\xi-8.0998)} + \cdots + 19.9362e^{(-13.2450*\xi-7.2254)}, \tag{67}$$

Solution for $\beta = -0.3$:

$$\hat{\theta}(\xi) = 3.2064e^{(-1.6155*\xi-3.8584)} + \cdots + 19.7640e^{(-12.2351*\xi-8.2594)}, \tag{68}$$

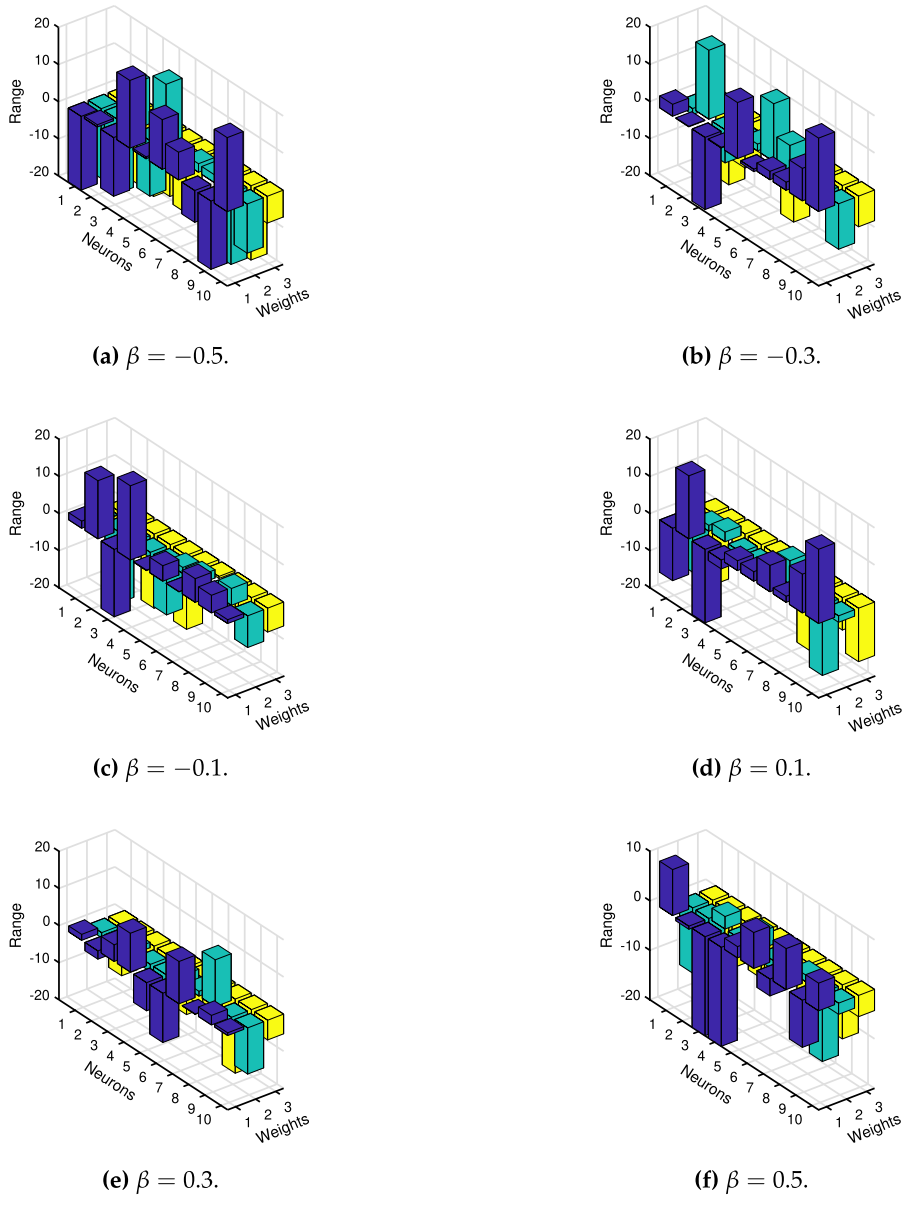

(a) $\beta = -0.5$. **(b)** $\beta = -0.3$.

(c) $\beta = -0.1$. **(d)** $\beta = 0.1$.

(e) $\beta = 0.3$. **(f)** $\beta = 0.5$.

Figure 14 Weights obtained by ANN–BHCS algorithm for case 5

Solution for $\beta = -0.1$:

$$\hat{\theta}(\xi) = 1.9312e^{(-0.1831*\xi-4.6329)} + \cdots + 1.0286e^{(-8.5327*\xi-6.4404)}, \tag{69}$$

Solution for $\beta = 0.1$:

$$\hat{\theta}(\xi) = -14.1166e^{(-13.8929*\xi-19.4453)} + \cdots + 19.9964e^{(-1.7336*\xi-14.4155)}, \tag{70}$$

Solution for $\beta = 0.3$:

$$\hat{\theta}(\xi) = 1.5998e^{(-1.3810*\xi-13.6786)} + \cdots + 0.7404e^{(-12.4352*\xi-5.3138)}, \tag{71}$$

Table 10 Solutions of case 5 for different values of β

ξ	$\beta = -0.5$	$\beta = -0.3$	$\beta = -0.1$	$\beta = 0.1$	$\beta = 0.3$	$\beta = 0.5$
0	0.201387	0.265899	0.32226	0.373055	0.420281	0.462251
0.1	0.206053	0.272621	0.329889	0.380834	0.42768	0.469289
0.2	0.219447	0.290303	0.349657	0.401147	0.44752	0.488327
0.3	0.240678	0.317813	0.380153	0.43241	0.478195	0.517834
0.4	0.270292	0.355711	0.421611	0.474484	0.519269	0.557226
0.5	0.309891	0.405493	0.474998	0.527796	0.570781	0.606294
0.6	0.361881	0.469591	0.541871	0.593134	0.633021	0.665029
0.7	0.429848	0.551788	0.624402	0.671579	0.706447	0.733545
0.8	0.5212	0.658144	0.725499	0.764461	0.791636	0.812039
0.9	0.66295	0.799284	0.849003	0.873339	0.889251	0.900762
1	0.997123	0.999929	1.000007	0.999976	1.000002	0.999994

Solution for $\beta = 0.5$:

$$\hat{\theta}(\xi) = 9.2817e^{(-13.1731*\xi-8.1456)} + \cdots + 5.5888e^{(-2.2593*\xi-4.2874)}. \tag{72}$$

Numerical solutions of case 5 for different values of β are given in Table 10 and Fig. 15(a). From Fig. 15(a), it is clear that the dimensionless temperature θ increases as the value of thermal conductivity β goes from −0.5 to 0.5. Convergence of the fitness values for case 5 is given in Fig. 15(b). Histograms of the fitness values for different values of β are given in Figs. 15(c)–15(h). The figures show that more than 90% of the fitness values are very close to zero, which shows the efficiency of the ANN–BHCS algorithm.

6.6 Case 6

In this case, we have taken $\nu = 1.5$, $\psi = 0.5$, and β is varied from −0.5 to 0.5 with step size of 0.2. Using these values, Eq. (6) becomes

$$\frac{d^{1.5}\theta}{d\xi^{1.5}} + \beta\theta\frac{d^2\theta}{d\xi^2} + \beta\left(\frac{d\theta}{d\xi}\right)^2 - (0.5)^2\theta = 0; \quad 0 \le \xi \le 1, \tag{73}$$

with boundary conditions

$$\theta'(0) = 0, \qquad \theta(1) = 1. \tag{74}$$

The fitness function for Eqs. (73) and (74) is given by

$$\begin{aligned} \min \quad E = {} & \frac{1}{11}\sum_{m=0}^{10}\left(\frac{d^{1.5}\hat{\theta}}{d\xi^{1.5}} + \beta\hat{\theta}\frac{d^2\hat{\theta}}{d\xi^2} + \beta\left(\frac{d\hat{\theta}}{d\xi}\right)^2 - (0.5)^2\hat{\theta}\right)^2 \\ & + \frac{1}{2}\left(\left(\hat{\theta}'(0)\right)^2 + \left(\hat{\theta}(1) - 1\right)^2\right). \end{aligned} \tag{75}$$

The ANN–BHCS algorithm is used to minimize the fitness function (75) for different values of β. The minimum fitness values for $\beta = -0.5, -0.3, -0.1, 0.1, 0.3$, and 0.5 are 1.1723E−06, 2.0482E−07, 3.9230E−08, 2.9632E−09, 2.2827E−10, and 4.3199E−11 respectively. Weights obtained to minimize the fitness function for different values of β are given in Fig. 16. Series solutions of case 6 with different values of β are given as follows:

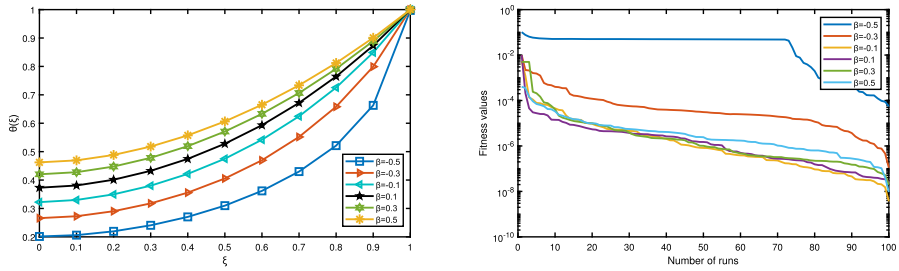

(a) Solutions for case 5. **(b)** Convergence of fitness values for case 5.

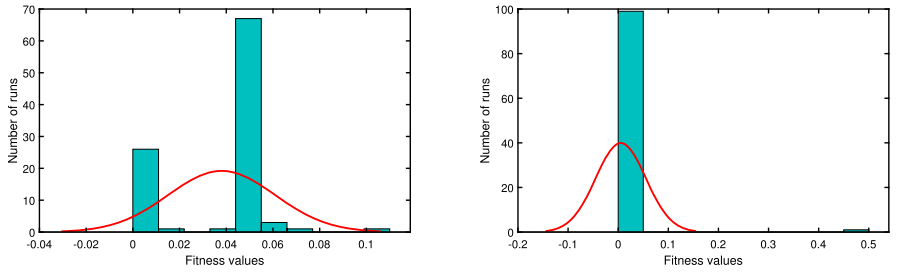

(c) $\beta = -0.5$. **(d)** $\beta = -0.3$.

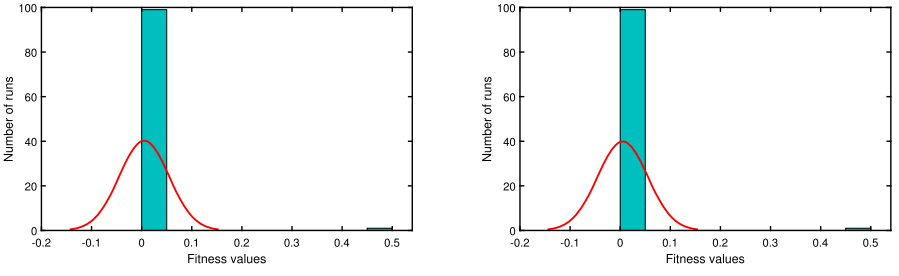

(e) $\beta = -0.1$. **(f)** $\beta = 0.1$.

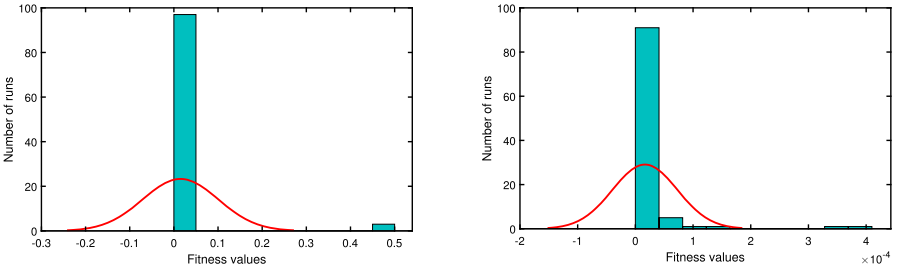

(g) $\beta = 0.3$. **(h)** $\beta = 0.5$.

Figure 15 Results obtained by ANN–BHCS algorithm for case 5

Solution for $\beta = -0.5$:

$$\hat{\theta}(\xi) = 42.9653e^{(-15.1854*\xi-10.0023)} + \cdots - 3.2385e^{(4.2429*\xi-9.0045)}, \tag{76}$$

Solution for $\beta = -0.3$:

$$\hat{\theta}(\xi) = -5.3645e^{(0.2792*\xi-2.1669)} + \cdots + 0.5784e^{(0.6436*\xi-0.1355)}, \tag{77}$$

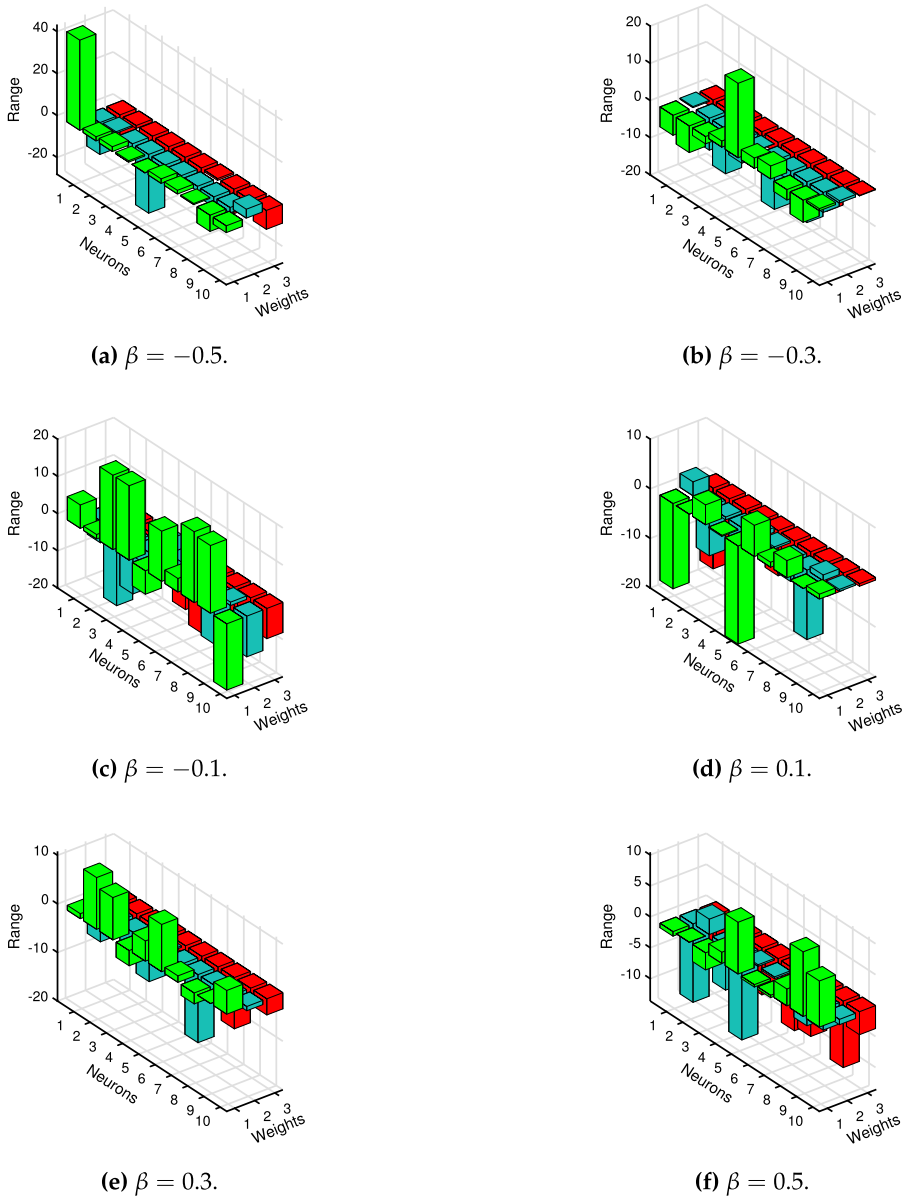

(a) $\beta = -0.5$. **(b)** $\beta = -0.3$.

(c) $\beta = -0.1$. **(d)** $\beta = 0.1$.

(e) $\beta = 0.3$. **(f)** $\beta = 0.5$.

Figure 16 Weights obtained by ANN–BHCS algorithm for case 6

Solution for $\beta = -0.1$:

$$\hat{\theta}(\xi) = 6.2815e^{(-5.9369*\xi-11.4495)} + \cdots - 17.7978e^{(-10.9295*\xi-8.1251)}, \tag{78}$$

Solution for $\beta = 0.1$:

$$\hat{\theta}(\xi) = -17.1800e^{(2.8172*\xi-16.2736)} + \cdots + 0.9790e^{(0.3888*\xi-0.5252)}, \tag{79}$$

Solution for $\beta = 0.3$:

$$\hat{\theta}(\xi) = 1.0322e^{(-6.3497*\xi-4.6384)} + \cdots + 4.8820e^{(-0.8769*\xi-3.3310)}, \tag{80}$$

Table 11 Solutions of case 6 for different values of β

ξ	$\beta = -0.5$	$\beta = -0.3$	$\beta = -0.1$	$\beta = 0.1$	$\beta = 0.3$	$\beta = 0.5$
0	0.692576	0.7711602	0.818874	0.85344025	0.87856631	0.897088726
0.1	0.701591	0.7782135	0.823855	0.85661451	0.88078124	0.898750233
0.2	0.717623	0.7912543	0.833969	0.86399013	0.88631954	0.903104574
0.3	0.737751	0.8074587	0.847053	0.87417662	0.89434646	0.909620598
0.4	0.762194	0.8265412	0.862613	0.88666314	0.90446989	0.918011396
0.5	0.791208	0.8483448	0.880408	0.90118365	0.91645402	0.928089048
0.6	0.824867	0.872818	0.900295	0.91756974	0.93013898	0.939718015
0.7	0.863052	0.9000391	0.922207	0.93570855	0.94541058	0.952795746
0.8	0.905427	0.9301718	0.946124	0.95552414	0.96218459	0.967242357
0.9	0.951382	0.9634192	0.972058	0.97696585	0.98039732	0.982994275
1	0.999915	0.9999989	1.000008	1.00000009	0.99999958	1.000000054

Solution for $\beta = 0.5$:

$$\hat{\theta}(\xi) = -0.7394e^{(-12.6785*\xi-7.3373)} + \cdots + 7.4517e^{(-0.8547*\xi-3.7189)}. \tag{81}$$

Numerical solutions of case 6 for different values of β are given in Table 11 and Fig. 17(a). From Fig. 17(a), it is clear that the dimensionless temperature θ increases as the value of thermal conductivity β goes from −0.5 to 0.5. Convergence of the fitness values for case 6 is given in Fig. 17(b). Histograms of the fitness values for different values of β are given in Figs. 17(c)–17(h). The figures show that more than 90% of the fitness values are very close to zero, which shows the efficiency of the ANN–BHCS algorithm.

6.7 Case 7

In this case, we have taken $\nu = 1.5$, $\psi = 1.5$, and β is varied from −0.5 to 0.5 with step size of 0.2. Using these values, Eq. (6) becomes

$$\frac{d^{1.5}\theta}{d\xi^{1.5}} + \beta\theta\frac{d^2\theta}{d\xi^2} + \beta\left(\frac{d\theta}{d\xi}\right)^2 - (1.5)^2\theta = 0; \quad 0 \le \xi \le 1, \tag{82}$$

with boundary conditions

$$\theta'(0) = 0, \qquad \theta(1) = 1. \tag{83}$$

The fitness function for Eqs. (82) and (83) is given by

$$\begin{aligned} \min \quad E = {} & \frac{1}{11}\sum_{m=0}^{10}\left(\frac{d^{1.5}\hat{\theta}}{d\xi^{1.5}} + \beta\hat{\theta}\frac{d^2\hat{\theta}}{d\xi^2} + \beta\left(\frac{d\hat{\theta}}{d\xi}\right)^2 - (1.5)^2\hat{\theta}\right)^2 \\ & + \frac{1}{2}\left(\left(\hat{\theta}'(0)\right)^2 + \left(\hat{\theta}(1) - 1\right)^2\right). \end{aligned} \tag{84}$$

The BHCS algorithm is used to minimize the fitness function (84) for different values of β. The minimum fitness values for $\beta = -0.5, -0.3, -0.1, 0.1, 0.3$, and 0.5 are 3.2749E−04, 6.1684E−06, 1.0813E−07, 6.9620E−08, 3.3707E−08, and 6.1241E−08 respectively. Weights obtained to minimize the fitness function for different values of β are given in Fig. 18. Series solutions of case 6 with different values of β are given as follows:

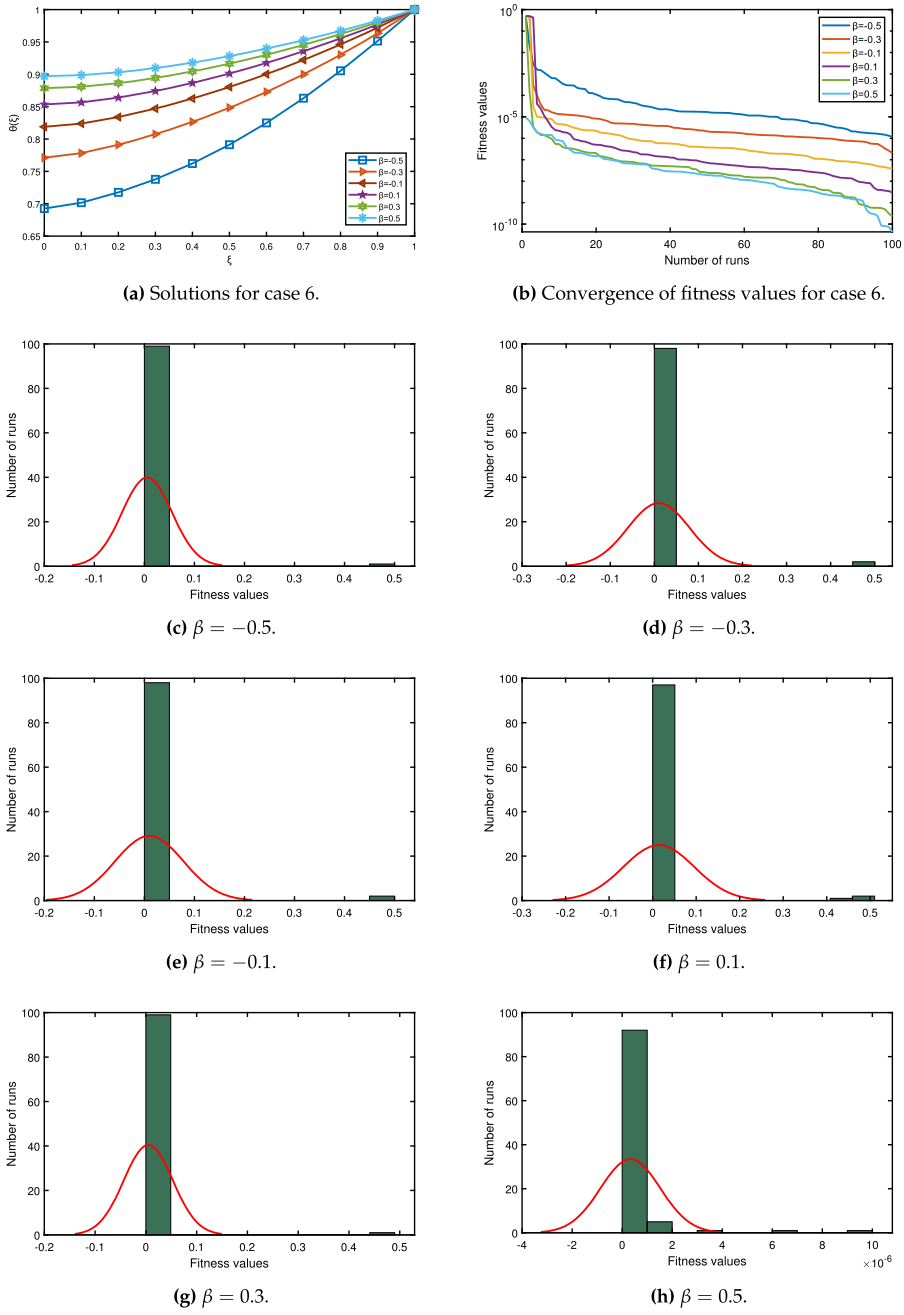

(a) Solutions for case 6.

(b) Convergence of fitness values for case 6.

(c) $\beta = -0.5$.

(d) $\beta = -0.3$.

(e) $\beta = -0.1$.

(f) $\beta = 0.1$.

(g) $\beta = 0.3$.

(h) $\beta = 0.5$.

Figure 17 Results obtained by ANN–BHCS algorithm for case 6

Solution for $\beta = -0.5$:

$$\hat{\theta}(\xi) = 0.0011e^{(-18.7295*\xi-12.1889)} + \cdots + 0.0036e^{(10.6494*\xi-4.9802)}, \tag{85}$$

Solution for $\beta = -0.3$:

$$\hat{\theta}(\xi) = 2.1083e^{(14.4756*\xi-16.5181)} + \cdots + 19.4106e^{(-14.7538*\xi-16.7618)}, \tag{86}$$

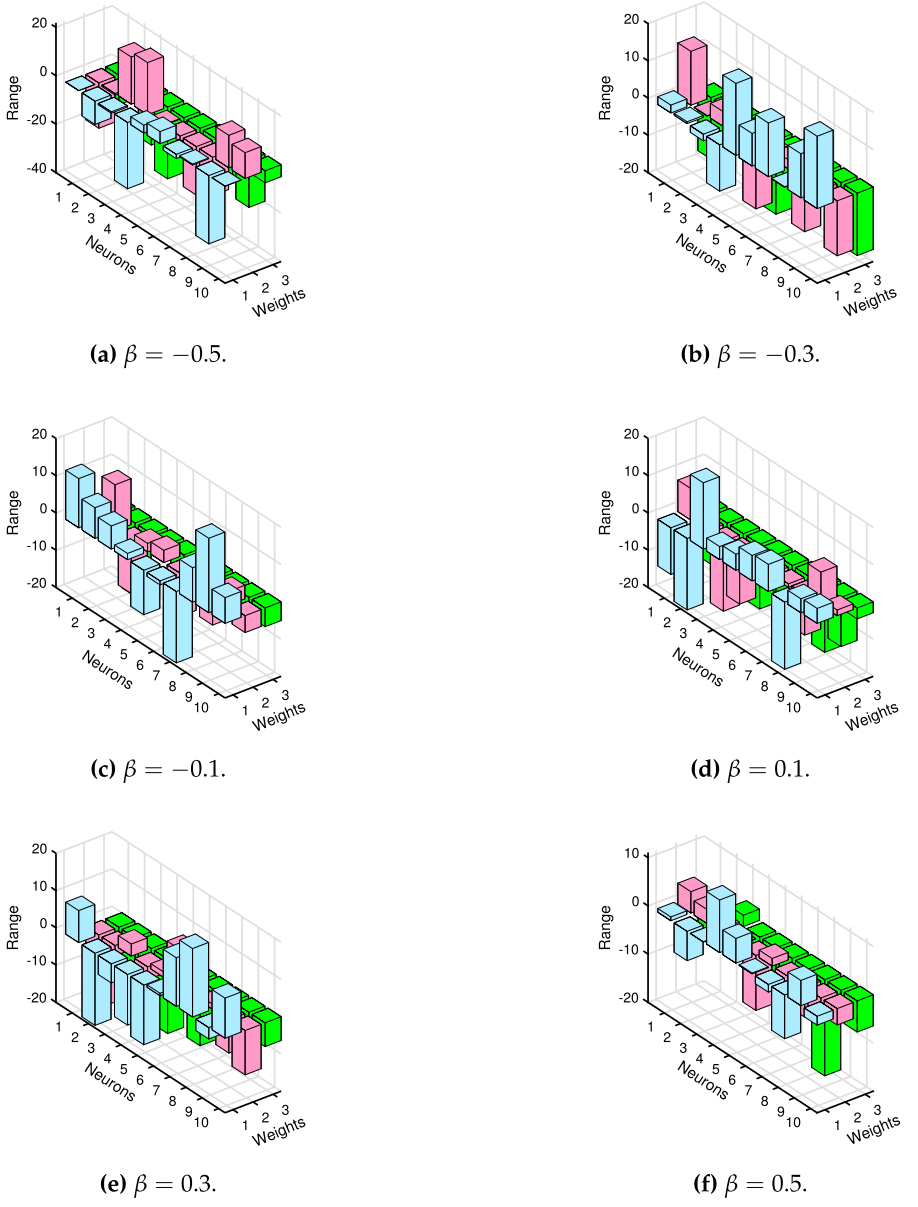

(a) $\beta = -0.5$. **(b)** $\beta = -0.3$.

(c) $\beta = -0.1$. **(d)** $\beta = 0.1$.

(e) $\beta = 0.3$. **(f)** $\beta = 0.5$.

Figure 18 Weights obtained by ANN–BHCS algorithm for case 7

Solution for $\beta = -0.1$:

$$\hat{\theta}(\xi) = 13.2030e^{(0.9806*\xi-4.6034)} + \cdots + 6.9143e^{(-4.5284*\xi-5.0134)}, \tag{87}$$

Solution for $\beta = 0.1$:

$$\hat{\theta}(\xi) = -12.5240e^{(8.4684*\xi-13.8879)} + \cdots + 4.0159e^{(1.5309\xi-2.9223)}, \tag{88}$$

Solution for $\beta = 0.3$:

$$\hat{\theta}(\xi) = 8.6030e^{(-19.6605*\xi-9.1743)} + \cdots + 10.7660e^{(-11.8943*\xi-6.3870)}, \tag{89}$$

Table 12 Solutions of case 7 for different values of β

ξ	$\beta = -0.5$	$\beta = -0.3$	$\beta = -0.1$	$\beta = 0.1$	$\beta = 0.3$	$\beta = 0.5$
0	0.102229	0.152917	0.236745	0.300268	0.356649	0.407166
0.1	0.1063	0.160234	0.247773	0.312229	0.367969	0.417422
0.2	0.117445	0.177101	0.272432	0.339384	0.394859	0.442789
0.3	0.134263	0.201217	0.307361	0.377666	0.433094	0.479401
0.4	0.155998	0.233131	0.352945	0.426662	0.481616	0.525858
0.5	0.183067	0.274508	0.410597	0.486878	0.540287	0.581629
0.6	0.218689	0.327975	0.482524	0.559267	0.609343	0.646549
0.7	0.273403	0.398064	0.571904	0.645121	0.689234	0.720658
0.8	0.376272	0.495288	0.68319	0.745998	0.780542	0.804112
0.9	0.594308	0.653159	0.8227	0.863658	0.883917	0.89714
1	0.999193	0.999995	1.000003	0.999997	1.000034	1.000005

Solution for $\beta = 0.5$:

$$\hat{\theta}(\xi) = 0.7823e^{(4.4278*\xi-8.2779)} + \cdots - 1.8288e^{(-3.3932*\xi-6.4575)}. \tag{90}$$

Numerical solutions for case 7 are given in Table 12. Solutions are also plotted in Fig. 19(a) for different values of β. The solution figures show that dimensionless temperature θ increases with increasing the values of thermal conductivity from −0.5 to 0.5. Convergence of the fitness values for case 7 is given in Fig. 19(b). Histograms for the fitness values for different values of β are plotted in Figs. 19(c)–19(h).

7 Sensitivity analysis of parameters

In this section, we analyze the sensitivity of different parameters which are number of neurons, population size, and discovery probability *pa*. The ODE in case 1 with $\psi = 0.2$ is solved for sensitivity analysis of parameters. Solutions and absolute errors for different values of parameters are given in Tables 13, 14, 15, 16, 17, 18. We have solved the problem for 3, 5, and 10 neurons with fixed population size of 50 and discovery probability $pa = 0.3$, and the results show that the ANN–BHCS algorithm gives better solution for 10 neurons. The problem is solved for different values of discovery probability $pa = 0.01, 0.15$, and 0.3, and the number of neurons and population size were fixed as 10 and 50 respectively. For $pa = 0.3$, the ANN–BHCS algorithm gives better solution. Similarly, the problem is solved for different population sizes, and the results show that for 50 population size the algorithm gives better results.

8 Conclusion

In this paper, we have used ANN-based biogeography-based heterogeneous cuckoo search algorithm (ANN–BHCS) to analyze the problem of temperature distribution for convective straight fins. The ANN–BHCS algorithm is an efficient technique for the solution of fractional differential equations. We have considered seven cases of the problem, in which three cases are of integer order and four cases are of fractional order. In the first case, we have solved integer order energy balance equation for different values of thermogeometric fin parameter ψ. The series solutions for case 1 are given in Eqs. (34), (35) and (36). The comparison of exact and numerical solutions obtained by HPM, VIM, HPSTM, and ANN–BHCS for case 1 is given in Tables 1–6. Solutions obtained for case 1 are also plotted in Fig. 5(a). The results show that the ANN–BHCS algorithm gives better solutions

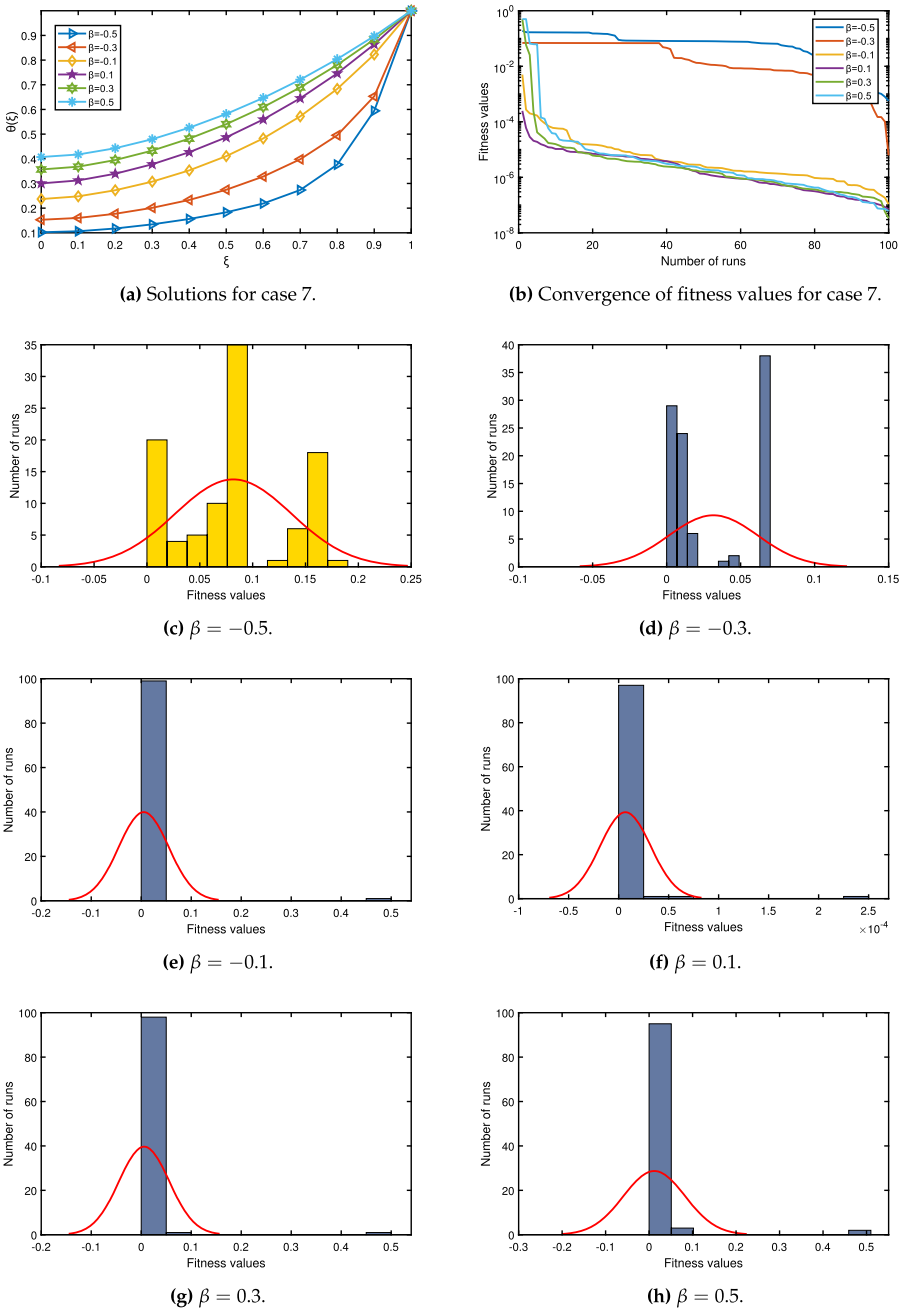

(a) Solutions for case 7.

(b) Convergence of fitness values for case 7.

(c) $\beta = -0.5$.

(d) $\beta = -0.3$.

(e) $\beta = -0.1$.

(f) $\beta = 0.1$.

(g) $\beta = 0.3$.

(h) $\beta = 0.5$.

Figure 19 Results obtained by ANN–BHCS algorithm for case 7

than other techniques. The efficiency of the algorithm is also obvious from the histograms of MAD, TIC, and ENSE values for case 1 in Figs. 6 and 7. From the second to seventh case, we have taken $\beta = -0.5, -0.3, -0.1, 0.1, 0.3, 0.5$ for all the cases. In the second and third case, we have considered integer order energy balance equation. Series solutions for the second and third case are given in Eqs. (40)–(45) and (49)–(54). Numerical solutions for the second and third case are given in Tables 7 and 8. Solution plots and histograms for fitness values of second and third case are given in Figs. 9 and 11. For both the cases,

Table 13 Solutions obtained for different number of neurons

ξ	Exact	$\hat{\theta}(\xi)$ (3 neurons)	$\hat{\theta}(\xi)$ (5 neurons)	$\hat{\theta}(\xi)$ (10 neurons)
0	0.98032800	0.98033066	0.98032478	0.980328074
0.1	0.98052407	0.98052777	0.98052085	0.980524147
0.2	0.98111236	0.98111760	0.98110934	0.981112432
0.3	0.98209312	0.98209990	0.98209052	0.982093168
0.4	0.98346672	0.98347472	0.98346462	0.983466756
0.5	0.98523372	0.98524237	0.98523202	0.985233752
0.6	0.98739483	0.98740350	0.98739332	0.987394863
0.7	0.98995091	0.98995901	0.98994944	0.989950948
0.8	0.99290299	0.99291012	0.99290158	0.992903022
0.9	0.99625224	0.99625835	0.99625110	0.99625226
1	1.00000000	1.00000551	0.99999934	1.000000005

Table 14 Absolute errors (AE) for different number of neurons

ξ	AE (3 neurons)	AE (5 neurons)	AE (10 neurons)
0	2.6613E–06	3.2195E–06	7.68E–08
0.1	3.6959E–06	3.2155E–06	7.71E–08
0.2	5.2352E–06	3.0270E–06	6.76E–08
0.3	6.7871E–06	2.6019E–06	5.06E–08
0.4	7.9974E–06	2.0990E–06	3.51E–08
0.5	8.6490E–06	1.7039E–06	2.79E–08
0.6	8.6620E–06	1.5105E–06	2.95E–08
0.7	8.0928E–06	1.4692E–06	3.41E–08
0.8	7.1344E–06	1.4090E–06	3.36E–08
0.9	6.1164E–06	1.1413E–06	2.25E–08
1	5.5052E–06	6.5876E–07	4.68E–09

Table 15 Solutions obtained for different values of discovery probability (*pa*)

ξ	Exact	$\hat{\theta}(\xi)$ ($pa = 0.01$)	$\hat{\theta}(\xi)$ ($pa = 0.15$)	$\hat{\theta}(\xi)$ ($pa = 0.3$)
0	0.98032800	0.98033472	0.98032852	0.980328074
0.1	0.98052407	0.98053054	0.98052459	0.980524147
0.2	0.98111236	0.98111799	0.98111282	0.981112432
0.3	0.98209312	0.98209766	0.98209346	0.982093168
0.4	0.98346672	0.98347050	0.98346697	0.983466756
0.5	0.98523372	0.98523725	0.98523392	0.985233752
0.6	0.98739483	0.98739841	0.98739504	0.987394863
0.7	0.98995091	0.98995441	0.98995115	0.989950948
0.8	0.99290299	0.99290589	0.99290322	0.992903022
0.9	0.99625224	0.99625393	0.99625240	0.99625226
1	1.00000000	1.00000029	1.00000006	1.000000005

Table 16 Absolute errors (AE) for different values of discovery probability (*pa*)

ξ	AE ($pa = 0.01$)	AE ($pa = 0.15$)	AE ($pa = 0.3$)
0	6.7251E–06	5.2275E–07	7.68E–08
0.1	6.4719E–06	5.1923E–07	7.71E–08
0.2	5.6209E–06	4.5620E–07	6.76E–08
0.3	4.5405E–06	3.4699E–07	5.06E–08
0.4	3.7794E–06	2.4833E–07	3.51E–08
0.5	3.5265E–06	2.0122E–07	2.79E–08
0.6	3.5732E–06	2.0787E–07	2.95E–08
0.7	3.4939E–06	2.3442E–07	3.41E–08
0.8	2.8993E–06	2.3147E–07	3.36E–08
0.9	1.6919E–06	1.6626E–07	2.25E–08
1	2.9361E–07	6.1897E–08	4.68E–09

Table 17 Solutions obtained for different population sizes

ξ	Exact	$\hat{\theta}(\xi)$ (pop = 20)	$\hat{\theta}(\xi)$ (pop = 30)	$\hat{\theta}(\xi)$ (pop = 50)
0	0.98032800	0.98034833	0.98032832	0.980328074
0.1	0.98052407	0.98054432	0.98052459	0.980524147
0.2	0.98111236	0.98112991	0.98111297	0.981112432
0.3	0.98209312	0.98210581	0.98209368	0.982093168
0.4	0.98346672	0.98347487	0.98346720	0.983466756
0.5	0.98523372	0.98523952	0.98523415	0.985233752
0.6	0.98739483	0.98740070	0.98739529	0.987394863
0.7	0.98995091	0.98995790	0.98995148	0.989950948
0.8	0.99290299	0.99290998	0.99290371	0.992903022
0.9	0.99625224	0.99625658	0.99625313	0.99625226
1	1.00000000	0.99999987	1.00000106	1.000000005

Table 18 Absolute errors (AE) for different population sizes

ξ	AE (pop = 20)	AE (pop = 30)	AE (pop = 50)
0	2.0333E–05	3.2537E–07	7.68E–08
0.1	2.0249E–05	5.1812E–07	7.71E–08
0.2	1.7547E–05	6.0088E–07	6.76E–08
0.3	1.2692E–05	5.6132E–07	5.06E–08
0.4	8.1468E–06	4.7660E–07	3.51E–08
0.5	5.7918E–06	4.2680E–07	2.79E–08
0.6	5.8618E–06	4.5634E–07	2.95E–08
0.7	6.9829E–06	5.6629E–07	3.41E–08
0.8	6.9949E–06	7.2607E–07	3.36E–08
0.9	4.3411E–06	8.9659E–07	2.25E–08
1	1.2613E–07	1.0598E–06	4.68E–09

the dimensionless temperature increases for the values of $\beta = -0.5, -0.3, -0.1, 0.1, 0.3, 0.5$. The cases from the fourth to seventh are of fractional order. The series solutions for all the cases are given in results section. Numerical solutions from the fourth to seventh case are given in Tables 9–12. Solution plots and histograms of fitness values for the fourth to seventh cases are given in Figs. 13, 15, 17 and 19. The results show that the ANN–BHCS algorithm can efficiently solve the integer and fractional order differential equations.

Acknowledgements
The authors acknowledge the support provided by the Department of Mathematics, Faculty of Science, King Mongkut's University of Technology Thonburi (KMUTT), 126 Pracha Uthit Rd., Bang Mod, Thung Khru, Bangkok 10140, Thailand.

Funding
The funding is provided by the Center of Excellence in Theoretical and Computational Science (TaCS-CoE), KMUTT.

Abbreviations
A_c, Cross section area; b, Length; P, Perimeter; T, Temperature; k_a, Thermal conductivity; *MLF*, Mittag-Leffler function; *pa*, Discovery probability; HSI, Habitat's suitability index; I,Immigration rate; E,Emigration rate; f, Activation function; j, Total number of neurons; α_i, β_i, ω_i, Unknown weights; $\hat{\theta}(\xi)$, Approximate series solution; E_1, Solution error of differential equation; E_2, Solution error of initial/boundary values; ANNs, Artificial neural networks; ODE, Ordinary differential equation; HPM, Homotopy perturbation method; VIM,Variational iteration method; HPSTM,Homotopy perturbation Sumudu transform method; BBO, Biogeography-based optimization; CS, Cuckoo search; BHCS, Biogeography based heterogeneous cuckoo search; TIC, Theil's inequality coefficient; MAD, Mean absolute deviation; NSE, Nash–Sutcliffe efficiency; ENSE, Error in Nash–Sutcliffe efficiency; AE, Absolute errors.

Availability of data and materials
The data that support the findings of this study are available from the corresponding author upon reasonable request.

Competing interests
The authors declare that they have no competing interests.

Authors' contributions
All authors have equal contribution in writing of this paper. All authors read and approved the final manuscript.

Author details
[1]Department of Mathematics, Abdul Wali Khan University, Mardan 23200, KP, Pakistan. [2]KMUTT Fixed Point Research Laboratory, KMUTT-Fixed Point Theory and Applications Research Group, SCL 802 Fixed Point Laboratory, Department of Mathematics, Faculty of Science, King Mongkut's University of Technology Thonburi (KMUTT), 126 Pracha Uthit Rd., Bang Mod, Thung Khru, Bangkok 10140, Thailand. [3]Department of Medical Research, China Medical University Hospital, China Medical University, Taichung 40402, Taiwan.

Publisher's Note

Received: 14 June 2021 Accepted: 28 July 2021 Published online: 18 August 2021

References

1. Ganji, D., Rajabi, A.: Assessment of homotopy–perturbation and perturbation methods in heat radiation equations. Int. Commun. Heat Mass Transf. **33**, 391–400 (2006)
2. Aziz, A., Nguyen, H.: Two-dimensional performance of convecting-radiating fins of different profile shapes. Wärme-Stoffübertrag. **28**, 481–487 (1993)
3. Cuce, E., Cuce, P.M.: Homotopy perturbation method for temperature distribution, fin efficiency and fin effectiveness of convective straight fins with temperature-dependent thermal conductivity. Proc. Inst. Mech. Eng., Part C, J. Mech. Eng. Sci. **227**, 1754–1760 (2013)
4. Kern, D., Kraus, A.: Extended Surface Heat Transfer. McGraw-Hill, New York (1972)
5. Domairry, G., Fazeli, M.: Homotopy analysis method to determine the fin efficiency of convective straight fins with temperature-dependent thermal conductivity. Commun. Nonlinear Sci. Numer. Simul. **14**, 489–499 (2009)
6. Chiu, C.H., et al.: A decomposition method for solving the convective longitudinal fins with variable thermal conductivity. Int. J. Heat Mass Transf. **45**, 2067–2075 (2002)
7. Chiu, C.H., Chen, C.K.: Application of Adomian's decomposition procedure to the analysis of convective-radiative fins. J. Heat Transf. **125**, 312–316 (2003)
8. Lesnic, D., Heggs, P.: A decomposition method for power-law fin-type problems. Int. Commun. Heat Mass Transf. **31**, 673–682 (2004)
9. Bartas, J., Sellers, W.:. Radiation fin effectiveness (1960)
10. Aziz, A., Enamul Huq, S.: Perturbation solution for convecting fin with variable thermal conductivity (1975)
11. Arslanturk, C.: Optimum design of space radiators with temperature-dependent thermal conductivity. Appl. Therm. Eng. **26**, 1149–1157 (2006)
12. Arslanturk, C.: Optimization of straight fins with a step change in thickness and variable thermal conductivity by homotopy perturbation method. J. Therm. Sci. Technol. **30**, 9–19 (2010)
13. Singh, J., Kumar, D., Kılıçman, A.: Homotopy perturbation method for fractional gas dynamics equation using Sumudu transform. Abstr. Appl. Anal. **2013** Article ID 934060 (2013)
14. Ghorbani, A.: Beyond Adomian polynomials: He polynomials. Chaos Solitons Fractals **39**, 1486–1492 (2009)
15. Miller, K.S., Ross, B.: An Introduction to the Fractional Calculus and Fractional Differential Equations. Wiley, New York (1993)
16. Podlubny, I.: Fractional Differential Equations: An Introduction to Fractional Derivatives, Fractional Differential Equations, to Methods of Their Solution and Some of Their Applications. Elsevier, Amsterdam (1998)
17. Saha Ray, S., Poddar, B., Bera, R.: Analytical solution of a dynamic system containing fractional derivative of order one-half by Adomian decomposition method. J. Appl. Mech. **72**, 290–295 (2005)
18. Ray, S.S., Bera, R.: An approximate solution of a nonlinear fractional differential equation by Adomian decomposition method. Appl. Math. Comput. **167**, 561–571 (2005)
19. Ray, S.S., Bera, R.: Analytical solution of a fractional diffusion equation by Adomian decomposition method. Appl. Math. Comput. **174**, 329–336 (2006)
20. Ray, S.S.: A new approach for the application of Adomian decomposition method for the solution of fractional space diffusion equation with insulated ends. Appl. Math. Comput. **202**, 544–549 (2008)
21. Patra, A., Ray, S.S.: Analysis for fin efficiency with temperature-dependent thermal conductivity of fractional order energy balance equation using HPST method. Alex. Eng. J. **55**, 77–85 (2016)
22. Inan, B., Osman, M.S., Ak, T., Baleanu, D.: Analytical and numerical solutions of mathematical biology models: the Newell–Whitehead–Segel and Allen–Cahn equations. Math. Methods Appl. Sci. **43**, 2588–2600 (2020)
23. Park, C., Nuruddeen, R., Ali, K.K., Muhammad, L., Osman, M., Baleanu, D.: Novel hyperbolic and exponential ansatz methods to the fractional fifth-order Korteweg–de Vries equations. Adv. Differ. Equ. **2020**, 627 (2020)
24. Ali, K.K., Abd El Salam, M.A., Mohamed, E.M., Samet, B., Kumar, S., Osman, M.: Numerical solution for generalized nonlinear fractional integro-differential equations with linear functional arguments using Chebyshev series. Adv. Differ. Equ. **2020**, 494 (2020)
25. Ali, K.K., Cattani, C., Gómez-Aguilar, J., Baleanu, D., Osman, M.: Analytical and numerical study of the DNA dynamics arising in oscillator-chain of Peyrard–Bishop model. Chaos Solitons Fractals **139**, 110089 (2020)
26. Arqub, O.A., Osman, M.S., Abdel-Aty, A.H., Mohamed, A.B.A., Momani, S.: A numerical algorithm for the solutions of ABC singular Lane–Emden type models arising in astrophysics using reproducing kernel discretization method. Mathematics **8**, 923 (2020)
27. Dhawan, S., Machado, J.A.T., Brzeziński, D.W., Osman, M.S.: A Chebyshev wavelet collocation method for some types of differential problems. Symmetry **13**, 536 (2021)
28. Kumar, S., Kumar, R., Osman, M., Samet, B.: A wavelet based numerical scheme for fractional order SEIR epidemic of measles by using Genocchi polynomials. Numer. Methods Partial Differ. Equ. **37**, 1250–1268 (2021)

29. Bayones, F., Nisar, K.S., Khan, K.A., Raza, N., Hussien, N.S., Osman, M., Abualnaja, K.M.: Magneto-hydrodynamics (MHD) flow analysis with mixed convection moves through a stretching surface. AIP Adv. **11**, 045001 (2021)
30. Cuahutenango-Barro, B., Taneco-Hernández, M., Lv, Y.P., Gómez-Aguilar, J., Osman, M., Jahanshahi, H., Aly, A.A.: Analytical solutions of fractional wave equation with memory effect using the fractional derivative with exponential kernel. Results Phys. **25**, 104148 (2021)
31. Djennadi, S., Shawagfeh, N., Osman, M.S., Gómez-Aguilar, J., Arqub, O.A., et al.: The Tikhonov regularization method for the inverse source problem of time fractional heat equation in the view of ABC-fractional technique. Phys. Scr. **96**, 094006 (2021)
32. Khalid, A., Rehan, A., Nisar, K.S., Osman, M.S.: Splines solutions of boundary value problems that arises in sculpturing electrical process of motors with two rotating mechanism circuit. Phys. Scr. **96**, 104001 (2021)
33. Huang, W., Jiang, T., Zhang, X., Khan, N.A., Sulaiman, M.: Analysis of beam-column designs by varying axial load with internal forces and bending rigidity using a new soft computing technique. Complexity **2021**, Article ID 6639032 (2021)
34. Zhang, Y., Lin, J., Hu, Z., Khan, N.A., Sulaiman, M.: Analysis of third-order nonlinear multi-singular Emden–Fowler equation by using the LeNN-WOA-NM algorithm. IEEE Access **9**, 72111–72138 (2021). https://doi.org/10.1109/ACCESS.2021.3078750
35. Khan, N.A., Sulaiman, M., Kumam, P., Aljohani, A.J.: A new soft computing approach for studying the wire coating dynamics with Oldroyd 8-constant fluid. Phys. Fluids **33**, 036117 (2021)
36. Ahmad, A., Sulaiman, M., Aljohani, A.J., Alhindi, A., Alrabaiah, H.: Design of an efficient algorithm for solution of Bratu differential equations. Ain Shams Eng. J. **12**, 2211–2225 (2021)
37. Ahmad, A., Sulaiman, M., Alhindi, A., Aljohani, A.J.: Analysis of temperature profiles in longitudinal fin designs by a novel neuroevolutionary approach. IEEE Access **8**, 113285–113308 (2020)
38. Waseem, W., Sulaiman, M., Islam, S., Kumam, P., Nawaz, R., Raja, M.A.Z., Farooq, M., Shoaib, M.: A study of changes in temperature profile of porous fin model using cuckoo search algorithm. Alex. Eng. J. **59**, 11–24 (2020)
39. Bukhari, A.H., Sulaiman, M., Islam, S., Shoaib, M., Kumam, P., Raja, M.A.Z.: Neuro-fuzzy modeling and prediction of summer precipitation with application to different meteorological stations. Alex. Eng. J. **59**, 101–116 (2020)
40. Bukhari, A.H., Raja, M.A.Z., Sulaiman, M., Islam, S., Shoaib, M., Kumam, P.: Fractional neuro-sequential ARFIMA-LSTM for financial market forecasting. IEEE Access **8**, 71326–71338 (2020)
41. Waseem, W., Sulaiman, M., Alhindi, A., Alhakami, H.: A soft computing approach based on fractional order DPSO algorithm designed to solve the corneal model for eye surgery. IEEE Access **8**, 61576–61592 (2020)
42. Bukhari, A.H., Sulaiman, M., Raja, M.A.Z., Islam, S., Shoaib, M., Kumam, P.: Design of a hybrid NAR-RBFs neural network for nonlinear dusty plasma system. Alex. Eng. J. **59**, 3325–3345 (2020)
43. Khan, A., Sulaiman, M., Alhakami, H., Alhindi, A.: Analysis of oscillatory behavior of heart by using a novel neuroevolutionary approach. IEEE Access **8**, 86674–86695 (2020)
44. Waseem, W., Sulaiman, M., Kumam, P., Shoaib, M., Raja, M.A.Z., Islam, S.: Investigation of singular ordinary differential equations by a neuroevolutionary approach. PLoS ONE **15**, e0235829 (2020)
45. Waseem, W., Sulaiman, M., Aljohani, A.J.: Investigation of fractional models of damping material by a neuroevolutionary approach. Chaos Solitons Fractals **140**, 110198 (2020)
46. Ahmad, S., Sulaiman, M., Kumam, P., Hussain, Z., Asif Jan, M., Mashwani, W.K., Ullah, M.: A novel population initialization strategy for accelerating Levy flights based multi-verse optimizer. J. Intell. Fuzzy Syst. **39**, 1–17 (2020). https://doi.org/10.3233/JIFS-190112
47. Sulaiman, M., Ahmad, S., Iqbal, J., Khan, A., Khan, R.: Optimal operation of the hybrid electricity generation system using multiverse optimization algorithm. Comput. Intell. Neurosci. **2019**, Article ID 6192980 (2019)
48. Sulaiman, M., Ahmad, A., Khan, A., Muhammad, S.: Hybridized symbiotic organism search algorithm for the optimal operation of directional overcurrent relays. Complexity **2018**, Article ID 4605769 (2018)
49. Sulaiman, M., Waseem, Muhammad, S., Khan, A.: Improved solutions for the optimal coordination of DOCRs using firefly algorithm. Complexity **2018**, Article ID 7039790 (2018)
50. Sulaiman, M., Salhi, A., Khan, A., Muhammad, S., Khan, W.: On the theoretical analysis of the plant propagation algorithms. Math. Probl. Eng. **2018**, Article ID 6357935 (2018)
51. Sulaiman, M., Salhi, A., Selamoglu, B.I., Kirikchi, O.B.: A plant propagation algorithm for constrained engineering optimisation problems. Math. Probl. Eng. **2014**, Article ID 627416 (2014)
52. Coşkun, S.B., Atay, M.T.: Analysis of convective straight and radial fins with temperature-dependent thermal conductivity using variational iteration method with comparison with respect to finite element analysis. Math. Probl. Eng. **2007**, Article ID 042072 (2007)
53. Arslanturk, C.: A decomposition method for fin efficiency of convective straight fins with temperature-dependent thermal conductivity. Int. Commun. Heat Mass Transf. **32**, 831–841 (2005)
54. Oldham, K., Spanier, J.: The Fractional Calculus Theory and Applications of Differentiation and Integration to Arbitrary Order. Elsevier, Amsterdam (1974)
55. Kilbas, A.A., Srivastava, H.M., Trujillo, J.J.: Theory and Applications of Fractional Differential Equations, vol. 204. Elsevier, Amsterdam (2006)
56. Caputo, M.: Linear models of dissipation whose Q is almost frequency independent—II. Geophys. J. Int. **13**, 529–539 (1967)
57. Diethelm, K., Ford, N.J.: Multi-order fractional differential equations and their numerical solution. Appl. Math. Comput. **154**, 621–640 (2004)
58. Mainardi, F., Gorenflo, R.: The Mittag-Leffler function in the Riemann–Liouville fractional calculus. In: Boundary Value Problems, Special Functions and Fractional Calculus, pp. 215–225 (1996)
59. Yang, X.S., Deb, S.: Cuckoo search via Lévy flights. In: 2009 World Congress on Nature & Biologically Inspired Computing (NaBIC), pp. 210–214. IEEE Press, New York (2009)
60. Ding, X., Xu, Z., Cheung, N.J., Liu, X.: Parameter estimation of Takagi–Sugeno fuzzy system using heterogeneous cuckoo search algorithm. Neurocomputing **151**, 1332–1342 (2015)
61. Yang, X.S., Deb, S.: Engineering optimisation by cuckoo search. Int. J. Math. Model. Numer. Optim. **1**, 330–343 (2010)
62. Simon, D.: Biogeography-based optimization. IEEE Trans. Evol. Comput. **12**, 702–713 (2008)
63. Cheung, N.J., Ding, X.M., Shen, H.B.: A nonhomogeneous cuckoo search algorithm based on quantum mechanism for real parameter optimization. IEEE Trans. Cybern. **47**, 391–402 (2016)